TÉCNICO LISBOA

Cuffless Blood Pressure Estimation for Continuous 24/7 Patient Monitoring

Maria Margarida Almeirão Brites

Thesis to obtain the Master of Science Degree in

Biomedical Engineering

Supervisors: Prof. Helge Bjarup Dissing Sørensen
Prof. Agostinho Cláudio da Rosa

Examination Committee

Chairperson: Prof. João Miguel Raposo Sanches
Supervisor: Prof. Helge Bjarup Dissing Sørensen
Member of the Committee: Prof. Ana Luísa Nobre Fred

January 2021

Preface

The project developed for this thesis was a result of working in the Wireless Accessment of Respiratory and circulatory Distress (WARD) project - a collaborate research between two hospitals in the Capital Region of Denmark (Bispebjerg Hospital and Rigshospitalet) and the Biomedical Signal Processing Research Group at the Technical University of Denmark . This thesis presents the results obtained in the development of a cuffless blood pressure estimation algorithm at the Technical University of Denmark, Department of Health Technology. It was carried out from February the 3rd to August the 3rd 2020.

Declaration

I declare that this document is an original work of my own authorship and that it fulfills all the requirements of the Code of Conduct and Good Practices of the Universidade de Lisboa.

Acknowledgments

First I would like to thank my supervisors Helge B. D. Sørensen and Agostinho Cláudio da Rosa for giving me the possibility of working in this project. I would also like to thank professor Helge B. D. Sørensen for sharing his knowledge about science communication and providing guidance and support throughout the project.

I wish to thank Søren Møller Rasmussen for suggesting this interesting research topic, for helping me with the project details and providing motivating feedback to my work. His guidance and help are greatly appreciated.I would also like to thank the WARD team for welcoming me to the project, and particular to Søren Møller Rasmussen, Ying Gu and Birgit Agerholm Larsen who have from the beginning welcomed me to the group and to the offices at DTU.

Lastly, I thank my family and friends for supporting me over the last few months and giving me motivation to continue even when difficulties appear.

Abstract

Blood pressure (BP) is an important factor in the monitoring of patients admitted to the general ward, which is the focus of the Wireless Assessment of Respiratory and Circulatory Distress (WARD) clinical support system. Current practice relies on intermittent cuff based measurements, based on the oscillometric method. This method has major drawbacks such as the low frequency of evaluation and discomfort for the patients. Continuous cuffless blood pressure estimation methods have been explored in the literature as solutions for these problems. This master thesis aims at addressing cuffless blood pressure estimation using a data-driven method based on a machine learning algorithm (Random Forest).

Several morphological features and pulse arrival time features were extracted from the photoplethysmogram (PPG) waveform, its derivative and second derivative and from the ECG waveform. The set of features was used to train two Random Forest Regression models to estimate systolic blood pressure (SBP) and diastolic blood pressure (DBP), respectively. The BP estimation algorithm was fist trained and tested on data publicly available at the Multi-Parameter Intelligent Monitoring for Intensive Care II (MIMIC II) database. On a second stage, the solution was applied to data from the WARD project.

Although signal quality created difficulties in achieving results that compare to those in the literature, in a small subset of high quality data from the MIMIC II database, it was possible to obtain SBP and DBP estimations with a mean error of $5.20 \pm 5.13 mmHg$ and $1.70 \pm 7.98 mmHg$, respectively. The results obtained in the WARD data suggest the signal pre-processing and cleaning pipeline should be improved to meet the clinical standards. Despite the limitations, a machine learning method based on PPG and ECG features shows potential for the estimation of blood pressure without a cuff.

Keywords

Blood Pressure, Cuffless, Patient monitoring, Photoplethysmography, Electrocardiogram, Random Forest

Resumo

A pressão arterial é um fator importante na monitorização de doentes em enfermaria e é um dos sinais fisiológicos avaliados pelo sistema Wireless Assessment of Respiratory and Circulatory Distress (WARD) de apoio clínico. Atualmente, a monitorização é intermitente, e realizada com recurso a um esfigmomanómetro. Este método apresenta várias desvantagens, nomeadamente a baixa frequência das medições e o desconforto causado aos doentes. Diversos métodos alternativos foram estudados na literatura para a medição da pressão sanguínea de forma contínua e sem recurso a uma braçadeira insuflável. Esta dissertação visa abordar estes mesmos estudos e implementar um método de obtenção da pressão arterial com base num algoritmo de aprendizagem automática.

Um conjunto de *features* morfológicas e temporais foram calculadas dos sinais de PPG e ECG e posteriormente usadas para treinar dois modelos de Random Forest Regression para estimar a pressão arterial sistólica e diastólica, respetivamente. Os modelos foram treinados e testados em primeiro lugar a partir da base de dados pública Multi-Parameter Intelligent Monitoring for Intensive Care II (MIMIC II). Posteriormente, a solução desenvolvida foi aplicada aos dados do projeto WARD.

Embora a insuficiente qualidade dos sinais tenha dificultado a obtenção de resultados comparáveis aos da literatura, foi ainda assim possível obter valores de pressão arterial sistólica e diastólica com erro médio de $5.20 \pm 5.13 mmHg$ e $1.70 \pm 7.98 mmHg$, respetivamente, num subconjunto de dados da base de dados MIMIC II. Os resultados obtidos com os dados do projeto WARD sugerem que as etapas de remoção de ruído e artefactos e pré-processamento dos sinais devem ser melhoradas de modo a respeitar os padrões clínicos. Apesar das limitações, um algoritmo de aprendizagem automática baseado nos sinais de PPG e ECG demonstra potencial para a medição indireta da pressão arterial.

Palavras Chave

Pressão Arterial, Monitorização de doentes, Fotopletismografia, Eletrocardiograma, Aprendizagem Automática

Contents

List of Figures

List of Tables

Acronyms

AAMI	Advancement of Medical Instrumentation
ABP	Arterial Blood Pressure
BHS	British Hypertension Society
BP	Blood Pressure
COPD	Chronic Obstructive Pulmonary Disease
DBP	Diastolic Blood Pressure
ECG	Electrocardiogram
EWS	Early Warning Score
HR	Heart Rate
ICU	Intensive Care Unit
LOSO	Leave One Subject Out
MAE	Mean Absolute Error
MAP	Mean Arterial Pressure
ME	Mean Error
PAT	Pulse Arrival Time
PPG	Photoplethysmogram
PEP	Pre-Ejection Period
PP	Pulse Pressure
PTT	Pulse Transit Time
PWA	Pulse Wave Analysis
PWV	Pulse Wave Velocity
RMSE	Root Mean Square Error

RR	Respiratory Rate
SBP	Systolic Blood Pressure
STD	Standard Deviation
SpO_2	Peripheral Oxygen Saturation
WARD	Wireless Assessment of Respiratory and Circulatory Distress

1 Introduction

1.1 Problem Definition

Blood Pressure (BP) is a key hemodynamic variable, since subtle changes of its values, together with changes in other biosignals, are early signs of clinical deterioration eventually leading to adverse events [13]. Blood pressure is often monitored continuously in critically ill patients. It is common procedure to monitor Arterial Blood Pressure (ABP) by means of an arterial catheter during high-risk surgery, in the postoperative and in the Intensive Care Unit (ICU). The advantages of this monitoring technique include instantaneous detection of pressure changes and accuracy [14], as this is the gold standard method to monitor blood pressure [15]. However, this procedure is invasive, and may lead to complications so it is not suitable for general ward. Alternatively, blood pressure is often monitored using auscultation or oscillometry methods, which are non-invasive methods that employ an inflatable cuff [15].

Blood pressure is one of the biosignals being monitored in the Wireless Assessment of Respiratory and Circulatory Distress (WARD) project, which aims at developing a clinical monitoring system for early detection of patient deterioration and concerns general ward patients. In this project, signals are continuously measured from inpatients in the post operative period after major surgery and patients

admitted due to Chronic Obstructive Pulmonary Disease (COPD) exacerbation, using wear and forget devices. The biosignals acquired include Electrocardiogram (ECG), Photoplethysmogram (PPG) and blood pressure, among others.

Currently in the WARD project, Systolic Blood Pressure (SBP) and Diastolic Blood Pressure (DBP) are measured every 30 or 15 min during daytime and every hour or half hour from 10PM to 7AM using a cuff-based ambulatory blood pressure monitor. However, these measurements may cause discomfort to the patients and are disruptive during sleeping. A cuffless system for blood pressure estimation would allow unobtrusive and continuous measurements, providing more information about blood pressure variation.

Several systems have been proposed for continuous and cuffless blood pressure estimation. Many rely on Pulse Arrival Time (PAT) or Pulse Transit Time (PTT) measures, which consist of time differences obtained from two simultaneously acquired pulse signals representing the activity of the heart [15]. The electrocardiogram and photopletismogram waveforms acquired in the scope of the WARD project are commonly used to obtain such measures. Other systems which rely on features from the ECG and PPG waveforms separately have also been proposed. However, integration into clinical practice has not yet been achieved, possibly because the methods proposed either lack accuracy or validation over a sufficiently large population [16] [17]. Therefore, it is important to further improve and test these blood pressure estimation methods.

1.2 Project Goals

The main aim of the project is to investigate a method to estimate systolic and diastolic BP based on biosignals acquired in the scope of the WARD project, in a continuous or semi-continuous and unobtrusive manner. To do so, several goals were defined:

- Conduct state of the art research regarding existing cuffless blood pressure estimation methods and evaluate their outcomes based on existing standards for blood pressure devices, namely Advancement of Medical Instrumentation (AAMI) standard;
- Implement different state-of-the-art approaches for cuffless blood pressure estimation and test them on data available at the MIMIC database;
- Propose and test improvements to the current methods and compare the proposed method to reference methods for BP measurements;
- Apply the methods implemented to the large patient data set acquired in the WARD project, providing a more reliable validation compared to state of the art methods (which lack sufficient patient data for validation)

- Discuss the value of the development of a cuffless blood pressure device

1.3 Thesis Outline

Chapter 2: Presents a description of the WARD project including signal acquisition devices and data flow, and the research conducted. The relevance of continuous blood pressure estimation for this project is also discussed.

Chapter 3: Describes theory behind blood pressure measurements, including currently used methods and devices. Other concepts which are also useful for the understanding of this thesis are also described, namely the ECG and PPG signals and alternative and metrics from which blood pressure can potentially be estimated.

Chapter 4: Presents current state of the art in the field of continuous cuffless blood pressure estimation. This includes both methods based on physiological models and data-driven methods, using machine learning techniques. The most relevant literature methods found are discussed in detail.

Chapter 5: Describes the methods used in development of the blood pressure estimation algorithm. This includes data description and selection, signal processing, feature extraction and regression algorithm.

Chapter 6: Presents the obtained blood pressure estimation results obtained with one state of the art method implemented and the improved method developed. The two sets of data available are analysed and intermediate results obtained are also presented.

Chapter 7: Discusses the obtained results and performance of the blood pressure estimation methods, as well as and possible sources of error.

Chapter 8: Concludes the thesis and summarizes the most notable observations. In addition, future improvements are proposed and briefly discussed.

2

The WARD project

In this chapter, a description of the WARD project is presented. It includes signal acquisition devices and data flow, and the research conducted. The relevance of continuous blood pressure estimation for this project is also discussed.

2.1 Introduction

The Wireless Accessment of Respiratory and Circulatory Distress (WARD) project is a collaboration between the Technological University of Denmark (DTU), Rigshospitalet and Bispebjerg hospital which aims at conducting a continuous fully automatic assessment of vitals signal being monitored in high-risk patients.

The patients' biosignals are recorded using wear and forget devices and transmitted to a server in real time. Automatic signal processing algorithms then analyse these signals in order to detect abnormal values and access whether there is an event which could develop into a complication. In case of patient deterioration, the system notifies medical staff, so that it is possible to intervene at an early stage [1].

Currently, patients are monitored based on point wise measurements analysed according to the

Early Warning Score (EWS) standard [1]. However, the intermittent nature of this monitoring protocol potentiates undetected events, which could be detected by a continuous automatic monitoring system.

2.2 Early Warning Score protocol

This protocol consists of monitoring patients' vital signs at intervals that start at 12 hours and can be decreased in case there are abnormal values (called micro events) in the vital signs [18]. The vital signals measurements are scored on a scale from 0 to 3, and when one of the patient's parameters scores 3 or the patient has a cumulated score of more than 5, a specialist's clinical assessment is required, according to the algorithm used in the Capital Region of Denmark [19]. However, patients may deteriorate between measurements, meaning that deterioration will go undetected for hours, which may cause complications due to delay in diagnostic and intervention.

2.3 Continuous 24/7 monitoring

In a first stage of the project, continuous monitoring of vital signals was evaluated against EWS measurements in patients who had undergone major abdominal cancer surgery. The aim of this study was to compare the number of micro events identified by continuous monitoring to those detected by the standardized EWS. Peripheral Oxygen Saturation (SpO_2), Heart Rate (HR), Respiratory Rate (RR) were monitored by wearable devices in 50 patients. The results revealed that using continuous monitoring resulted in more severe micro events being detected compared to those detected by EWS [18].

In the automated response system developed by the WARD-project, 14 event classes have been defined by the medical doctors, including hypotension, circulatory failure and hypertension, among others. These events are based on abnormalities present in the vital signals for a predefined amount of time and should require intervention or assessment of the patient by a specialist [1].

The events can be used for two purposes. The first one is to trigger an alarm that alerts medical staff about the deterioration. The second is to use them as input of machine learning algorithms which aims at differentiating events that require medical interventions from those which do not require intervention. [1] This second approach was studied in the scope of the WARD project by Olsen et al. [20], in which events were classified in groups: *event requiring no attention*; *event requiring attention if repeated* and *event requiring immediate attention and correction*. The goal of the classification algorithm developed in this study was to detect early signs of deterioration using peripheral blood oxygenation, arterial blood pressure, perfusion index, heart rate and respiratory rate signs collected continuously. Compared to the alarm system based on single parameters, this algorithm resulted in a decreased number of false alarms and decreased missed early signs of deterioration [20].

At this point, 500 patients in the post operative period after abdominal cancer surgery and 200 patients admitted due to chronic COPD exacerbation have been monitored with WARD system's wear and forget devices, meaning that a large dataset is now available as a basis for algorithm development.

2.3.1 WARD equipment and data flow

The devices in the WARD system include an ECG sensor, a pulse oximeter, a BP monitor and a wristband sensor described in table 2.1.

ECG sensor	
Lifetouch Blue	ECG (10 seconds each minute) RR interval QRS amplitude HR (one minute average) respiration rate (RR)
Pulse Oximeter	
Nonin WristOx2	Oxygen Saturation PPG (10 seconds pr. minute) Pulse rate (PR)
BP monitor	
TM2441	SBP and DBP 1 measure every 15/30 min (daytime/nighttime) OR 1 measure every 30/60 min (daytime/nighttime)
Wristband sensor	
Empatica E4	electrodermal activity (EDA) Peripheral temperature 3D-acceleration PPG

Table 2.1: Devices included in the WARD system and respective signals measured. The pulse oximeter, BP monitor and device to acquire ECG are provided by Isansys.

Data from the sensors are wirelessly transmitted by bluetooth low energy (BLE) to the gateway, which sends the data to a server, as shown in figure 2.1. In the server data is then stored in a SQL-database, from which it can be extracted and processed. [1]

2.3.2 Continuous cuffless BP estimation

Some event classes, namely hypotension, circulatory failure and hypertension, are based on BP values. However, these measurements are currently performed intermittently using a cuff-based ambulatory blood pressure monitor (TM2441). During daytime measurements are performed once every 15 min

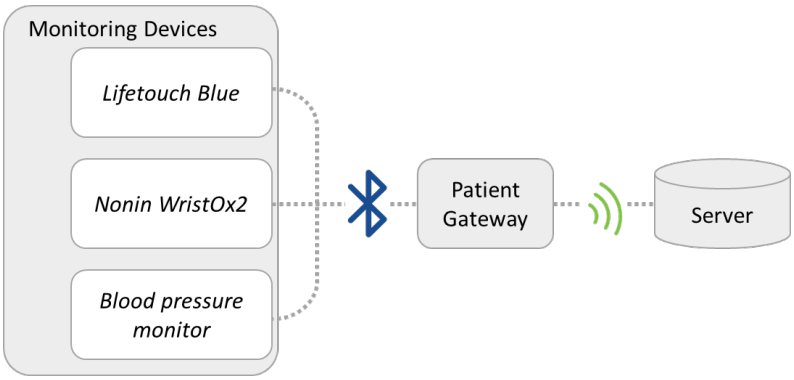

Figure 2.1: WARD system data flow. The signals are transmitted via Bluetooth to a table acting as gateway, from which data is sent to a local server at Rigshospitalet, where it is stored in a SQL database [1].

(or 30 min if uncomfortable for the patient) and from 10PM to 7AM BP is measured once every 30 min (or every hour if uncomfortable for the patient). However, the aim of the WARD system is to provide continuous monitoring which is not being achieved regarding blood pressure measurements with the current device.

The PPG and ECG signals are currently acquired each minute by the WARD system devices and several literature studies have shown that features extracted from these waveforms are promising for estimating blood pressure continuously [17] [16]. Therefore, using such blood pressure estimation methods would allow measurements of blood pressure to be performed on a minute basis. This continuous or more frequent blood pressure monitoring will allow events to be detected earlier and allow a faster intervention of the medical staff.

In addition, cuff based devices are cumbersome and uncomfortable for the patient, particularly during nighttime. In some cases, blood pressure measurements are even performed less often due to patient discomfort. Given that alternative methods to estimate blood pressure have been based on the PPG and ECG signals collected by the WARD system, replacing the ambulatory blood pressure monitor by these would decrease the apparatus required to monitor the patients.

The goal of this project is therefore to use the large dataset already acquired by the WARD devices to develop an algorithm for BP estimation based on alternative signals and test it against the cuff-based blood pressure monitor measurements.

3

Background Concepts

This chapter describes theory behind blood pressure measurements, including currently used methods and devices. Other concepts which are also useful for the understanding of this thesis are also described, namely the ECG and PPG signals and alternative and metrics from which blood pressure can potentially be estimated.

3.1 Blood Pressure

3.1.1 Definition

Blood pressure (BP) is the force exerted by the blood against any unit area of the vessel wall, and it is commonly expressed in millimeters of mercury (mmHg). This measurement unit originated from the measurements with the mercury manometer invented in 1846 by Poiseuille, which has since then been used as reference for measuring pressure. For instance, a pressure of 80mmHg means that the force exerted by the blood will push the column of mercury against gravity up to 80mm high [21].

Blood pressure consists of a series of pulse waves that correspond to heart cycles. The lowest point

of each pulse is called Diastolic Blood Pressure (DBP) and the pressure at the top of each pulse is the Systolic Blood Pressure (SBP). The difference between systolic and diastolic pressures is called Pulse Pressure (PP). [17] These points and the blood pressure waveform are represented in figure 3.1

Blood pressure is an important factor in the evaluation and diagnosis of multiple conditions such as stroke and cardiovascular disease, since hypertension is the most important modifiable risk factor for these diseases [22]. Therefore, several organizations have defined BP classifications to allow risk stratification. According to the American College of Cardiology [10], these categories are defined as in table 3.1.

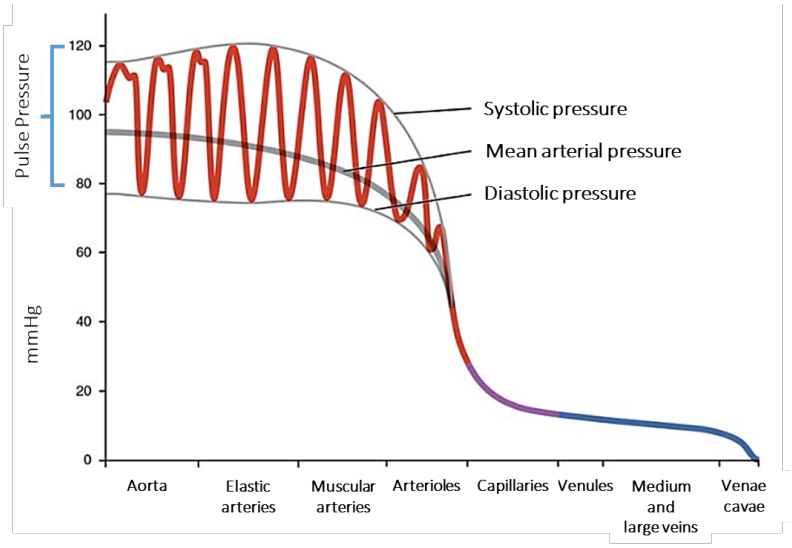

Figure 3.1: Representation of systolic, diastolic and mean blood pressures together with pulse pressure in the different portions of the circulatory system [2]

BP Category	SBP		DBP
Normal	< 120 mmHg	AND	< 80 mmHg
Elevated	$120 - 129$ mmHg	AND	< 80 mmHg
Stage 1 Hypertension	$130 - 139$ mmHg	OR	$80 - 89$ mmHg
Stage 2 Hypertension	> 140 mmHg	OR	> 90 mmHg

Table 3.1: Categories of BP in Adults [10]

3.1.2 Pulse pressure

In a healthy young adult, pulse pressure is around 40 mmHg [21]. However, it is commonly higher in healthy people following strenuous exercise or at an older age, when people frequently suffer from arteriosclerosis. Pulse pressure can also be lower than normal, in patients with congestive heart failure, stenosis of the aortic valve, or significant blood loss following trauma.

The pulse pressure is affected by two major factors, namely the stroke volume output of the heart and

the compliance (total distensibility) of the arterial tree [21]. A greater stroke volume output means that the pressure rise and fall during the cardiac cycle will be greater, and therefore the pulse pressure will be larger. On the contrary, pulse pressure is inversely proportional to the compliance of the arterial tree. The less compliant the arterial vessels are, the greater the rise in pressure for a given stroke volume of blood pumped into the arteries. Therefore, conditions such as arteriosclerosis, in which the arteries become hardened, cause an increase in the pulse pressure. [21]

3.1.3 Mean arterial pressure

The Mean Arterial Pressure (MAP) is the average of the arterial pressures measured over a cardiac cycle [17]. Since the portion of the cardiac cycle spent in diastole is larger than the period of systole, the arterial pressure remains closer to the diastolic pressure for longer than it remains close to to systolic pressure. For that reason, MAP is 60 percent determined by the diastolic pressure and 40 percent by the systolic pressure [21]. The mean arterial pressure is defined as:

$$MAP = \frac{2DBP + SBP}{3} \tag{3.1}$$

3.1.4 Methods to measure blood pressure

3.1.4.A Invasive Measurements

Arterial catheters, from which arterial blood pressure (ABP) waveforms are obtained, provide a direct measurement of blood pressure. Intra-arterial catheters are the standard of care for critically ill patients when it is necessary to perform continuous blood pressure monitoring and are commonly used during surgeries or in the ICU. This method consists of using an invasive catheter with an incorporated pressure transducer in fluid contact with blood at an arterial site, such as the radial artery or aorta. [17] [15]

The advantages of this invasive method are its accuracy and the fact that it provides continuous measurements and is clinically accepted. It is also accepted as a reliable reference method for validating new BP measurement technologies by regulatory agencies. [17] However, they are invasive and uncomfortable for the patient, and there is a possible risk of complications, such as infection and bleeding. In addition, experts are required to place and monitor the catheter site, and patients should be mostly stationary during monitoring [17].

3.1.4.B Auscultation

Auscultation is the standard clinical method for measuring blood pressure [15]. This method measures systolic and diastolic BP by occluding blood flow in an artery with a manual cuff and detecting the Korotkoff sounds using a stethoscope and manometer during cuff deflation [15]. Although auscultation is

accurate, clinically accepted and noninvasive its measurements are not continuous, and can be uncomfortable [17].

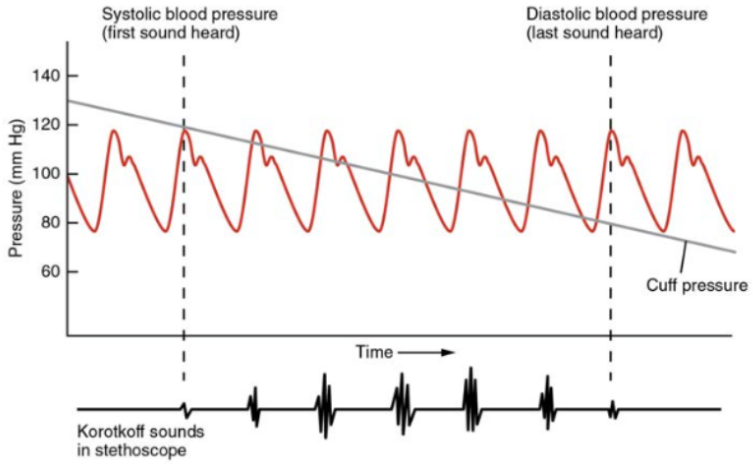

Figure 3.2: Illustration of auscultatory method for measuring systolic and diastolic arterial pressures: on the bottom the sounds heard throuhg a stethoscope placed over the antecubital artery are represented, together with the corresponding value of the arterial blood pressure (red curve) and cuff pressure (grey line) over time [2]

3.1.4.C Oscillometry

Oscillometry is an automatic technique based on the principle of occluding blood flow with an inflatable cuff with a pressure sensor inside it [17] [15].

The cuff is first inflated to a target pressure, which is typically between 160 mm Hg and 180 mm Hg on devices intended for adult use [23]. Once the cuff is inflated to the target pressure, its pressure is decreased in a controlled way up to a point below the DBP, as observed it the top trace on figure 3.3. At the same time, a series of small pressure pulses is being recorded [23]. The amplitude of these oscillometric pressure pulses is modulated by the difference between the MAP and the pressure applied in the cuff: it increases when the applied pressure is between the patient's diastolic blood pressure and MAP and decreases when the applied pressure is between MAP and systolic blood pressure [17]. This can be observed on the bottom trace in figure3.3.

Taking advantage of the waveform that results from varying the pulse amplitudes with applied pressure, SBP and DBP can be determined using empirically derived methods, such as the empirical fixed-ratios principle [15]

This method has some advantages when compared to auscultation. Namely, it easy to use and can easily be performed in ambulatory, it can be used in patients with muted Korotkoff sounds and it is less affected by external noise [3]. Additionally, it is not invasive, clinically accepted, with some oscillometric devices achieving BP errors within the AAMI limits of 5 mmHg bias and 8 mmHg precision [15]. How-

ever,these devices can be uncomfortable (particularly for frequent measurements), and inaccurate if not correctly used or not thoroughly validated [17].

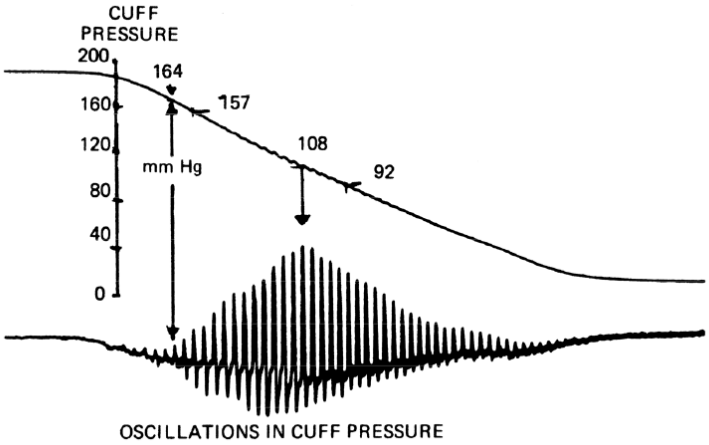

Figure 3.3: Representation of the oscillometric method. The top trace represents the cuff pressure and the bottom trace represents the oscillations in cuff pressure with respect to time. The maximal oscillation occurs at a pressure of 108 mm Hg, the mean arterial pressure. Adapted from [3].

3.1.4.D Volume Clamp

The volume clamp method is also known as vascular unloading or the method of Pẽnáz and it provides a noninvasive, continuous measurement of blood pressure [17]. It requires a finger cuff connected to a high-speed servo pump, together with a PPG sensor assembled on the finger, used to determine the total finger volume under an unloading cuff [24]. The high-speed servo controls the pressure applyed by the cuff, so that it cancels out the change of blood volume in the fingers with each cardiac cycle, maintaining it at a constant level. A continuous blood pressure waveform can then be obtained using an oscillometric calibration and empirical models [17].

An example of this technology is the Finapres non-invasive blood pressure (BP) monitor, which was introduced in the early 1980s [25]. It is based on the volume-clamp method, allowing a continuous beat-by-beat measurement of the arterial pressure waveform [17]. It measures the cuff pressure electronically and displays a signal corresponding to the arterial pressure waveform [24].

Volume clamp methods are noninvasive, continuous and automatic and have been used in research [15]. However, they can be inaccurate if not used correctly and the finger cuff can be uncomfortable for patients [17].

3.1.4.E Tonometry

Arterial tonometry provides a continuous and non invasive measurement of blood pressure and it does not require an inflatable cuff [17]. This method works by applying a transducer (manometer-tipped probe) on an artery and applying pressure so that the artery is flattened and the its wall tension is perpendicular to the transducer [15]. The transducer then measures the changes in arterial pressure with each cardiac cycle and these measurements are used to compute blood pressure.

Tonometry has been used in research [15] but it is very sensitive to motion, requires precise placement of the probe and frequent calibration, making it difficult to be used for routine measurements.

Despite being noninvasive continuous blood pressure measurement techniques, both tonometry and volume clamp techniques are intrusive because both require the application of external pressure or force on cuff during the entire course of the monitoring, which leads to discomfort and motion artifacts [17].

3.2 Photoplethysmography

PPG is a method for measuring the amount of light that is absorbed or reflected by blood vessels in living tissue [16].

The PPG device uses a light source, that emits light into the tissue, and a photodetector, which is the receptor of light that has interacted with the tissue. The PPG sensor can have two different configurations: in reflective mode, the photodetector is placed adjacent to the light source in reflection, whereas in transmission mode the photodetector is placed on one side of the tissue and the light source in the opposite side, as illustrated in figure 3.4. In this configuration, the emitted light is transmitted through the tissue, modulated by the underlying vasculature and then detected at the other side. This configuration is common in pulse oximeters designed to measure fingers and ear lobes [17].

The light source emits at a specific wavelength, which depends on final goal. Green light (565 nm) is commonly used for reflective PPG sensors, because the the maximum pulsatile component of reflected light occurs approximately in the range between 510 and 590 nm [9]. The red (680 nm) or near-infrared (810 nm) light is more commonly used for transmissive PPG devices, since it has more penetration depth. Since penetration depth is higher for infrared light compared to green light, it is more commonly used, as it reflects deep tissue blood pulse [9]. The use of PPG at multiple wavelengths is also routinely used in pulse oximetry, because the optical absorption of hemoglobin is a function of oxygenation, being different for oxyhemoglobin and deoxyhemoglobin [9].

The PPG signal has two major components, an AC component, also called pulsatile, and a DC component or non-pulsatile, as shown in figure 3.4. The AC component is related to blood volume variation that arises from heartbeats, whereas the DC component is a function of the stationary blood volume present in the tissue. This last component is influenced by respiration cycle, sympathetic nervous

system and thermoregulatory processes [25], that cause low frequency changes in the signal.

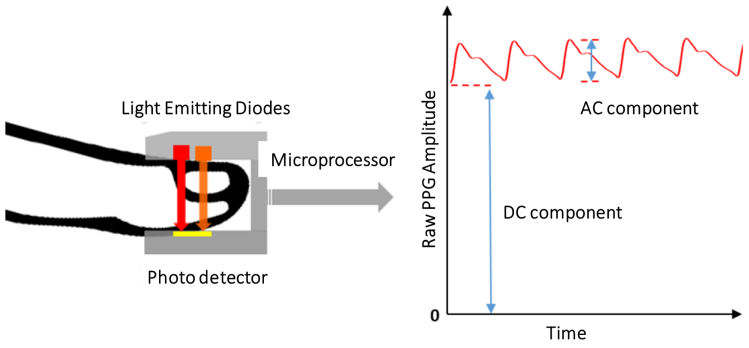

Figure 3.4: Illustration of instrumentation for PPG acquisition and PPG signal components. [4]

The AC component of the PPG waveform can be divided in two portions concerned respectively with systole and diastole. The rising edge, between the foot and the systolic peak of the pulse waveform is called anachrotic phase and is mainly connected with the contraction of the heart and therefore with systole [26]. The falling edge, also known as catacrotic phase, is concerned with diastole and wave reflections from the periphery [25]. A dicrotic notch can usually be identified in catacrotic phase of subjects with healthy compliant arteries [25]. The temporal delay between the systolic peak and diastolic peak in the PPG signal, as well as the temporal position of the dicrotic notch are influenced by several factors, such as the large artery stiffness, that normally is higher in older people. Due to this factor, the PPG waveform has slight differences between subjects, as exemplified in figure 3.5.

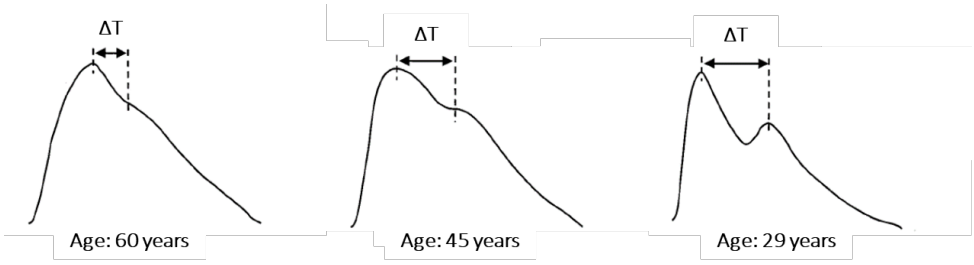

Figure 3.5: Changes in the PPG pulse characteristics with increasing age. ΔT is the temporal delay between the systolic peak and diastolic peak [5]

3.3 Electrocardiogram

An electrocardiogram is a recording of the electrical activity of the heart. The normal electrocardiogram is composed of a P wave, a QRS complex, and a T wave, as shown in figure 3.6. The QRS complex is typically composed by three distinct waves: the Q wave, the R wave, and the S wave [21]. Before atrial

contraction starts, the atria depolarize creating electrical potentials which give rise to the P wave. When the ventricles depolarize before contraction, electrical potentials are also generated and these generate the QRS complex. So, both the QRS complex components and the P wave are named depolarization waves, as they result from the spread of depolarization waves. The T wave is caused by potentials generated in the ventricular muscle after depolarization. Therefore the T wave is a repolarization wave. [21]

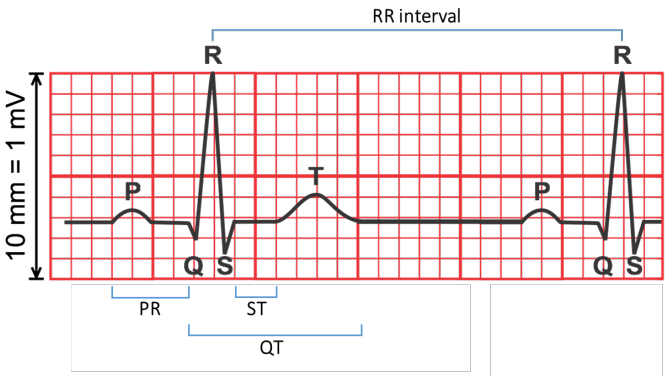

Figure 3.6: Normal electrocardiogram with waves and intervals represented.

3.4 Pulse Transit Time

Pulse Transit Time (PTT) is defined as the time that an arterial pressure wave requires to propagate along the walls of a given segment of the arterial tree [17]. It indirectly approximates Pulse Wave Velocity (PWV), the velocity at which an arterial pressure wave propagates along the walls of the arterial tree [17].

PWV reflects the properties of the arterial wall, namely arterial stiffness, and therefore varies with arterial pressure. PWV can be measured using the arrival time of a pressure wave propagating through the arterial tree in a certain distance between the proximal and distal arterial sites, in the form of PWV = L/PTT, where L is the distance between the proximal and distal sites. However, due to difficulties in the measurement of the distance L, PTT is used as a reciprocal measure. PTT can be derived from two pulse signals, including ECG and PPG [17].

The standard method to calibrate PTT estimates to BP values requires the definition of a mathematical model that relates PTT to BP in terms of unknown parameters. These parameters can then be obtained by measuring multiple pairs of PTT and BP values for each subject, allowing the construction of a calibration curve. [15]

The mathematical relationship between PTT and BP has been defined using empirical regression models and physical models. The first assume that the PTT is related to BP by means of a linear

function, quadratic function or other nonlinear functions. In the second case, the model is based on the theory of wave propagation in arteries.

3.4.1 Arterial Wave Propagation Models

The relationship between PTT and BP is based on two main equations for arterial wave propagation, the Moens–Korteweg equation and the relationship between the Young's modulus (E) and the arterial pressure (P) [17]. This last relation is given by:

$$E = E_0 e^{-\lambda P} \tag{3.2}$$

where E_0 is the Young's modulus at zero pressure, and λ is a coefficient that depends on the particular vessel.

The Moens–Korteweg equation determines the pressure's pulse wave velocity (PWV) as function of the the elasticity of arteries, and is given by:

$$PWV = \sqrt{\frac{Eh}{\rho d}} \tag{3.3}$$

where E is the Young's modulus, h is the arterial wall thickness, d is the artery's internal diameter, and ρ is the blood density.

The relationship between P and PWV can be derived by the Bramwell–Hill equation, which is obtained by combining equations 3.2 and 3.3 [17]:

$$PWV = \frac{L}{PTT} = \sqrt{\frac{hE_0 e^{-\lambda P}}{\rho d}} \tag{3.4}$$

where L is the length of the path traveled by the pulse wave. Several mathematical models have then been based on these equations to approximate the relationships between BP and the PTT. A popular example is to take the logarithmic relationship between BP and PTT from the the Bramwell–Hill equation, obtaining [27]:

$$P = \left(-\frac{2}{\lambda}\right) log(PPT) + \left(\frac{1}{\lambda}\right) log\left(\frac{\rho d L^2}{hE_0}\right) \tag{3.5}$$

The previous equation can be simplified as:

$$BP = A\, log(PTT) + B \tag{3.6}$$

Where A and B are subject-specific constants that can be obtained through the calibration procedure.

Other studies have presented models that linearly relate 1/PTT with BP, such as that given by [15]:

$$BP = \frac{A}{PTT} + B \tag{3.7}$$

One of the concerns regarding the application of a mathematical model is it is necessary to vary the BP over a considerable range to obtain the curve that can relate PTT to BP [17]. This curve can be constructed under different conditions that cause BP variations, such as exercising, hydrostatic posture, Valsalva maneuver, and medication [17]. Another problem is that, both PWV and PTT are not only affected by blood pressure but also by other factors, making this technique non-specific [17].

3.5 Pulse Arrival Time

Pulse arrival time (PAT) is defined as the time at which an arterial pressure wave arrives at a certain point of the arterial tree [17]. In other words, it corresponds to the time delay between the electrical activity of the heart and a peripheral pulse measured further down the arterial tree [17]. Therefore, PAT measurements require the measure of the electrical activity of the heart (typically using an electrocardiogram) and some measure of a mechanical activity of the pulse wave. The latter is typically performed using a photoplethysmogram, but it is also possible to use ballistocardiogram (BCG), seismocardiogram (SCG), and phonocardiogram (PCG) waveforms. [17]

Typically, PAT measurements consider as initial time reference the R-Wave of an ECG and as final reference a characteristic point of the PPG, such as the systolic peak.

The PAT interval includes the PTT interval plus the Pre-Ejection Period (PEP) delay [16]:

$$PAT = PTT + PEP \tag{3.8}$$

PEP is the pre-ejection period, which corresponds to the time needed to convert the electrical signal of the heart into a mechanical pumping force and isovolumetric contraction to open the aortic valve [17].

3.5.1 PAT vs. PTT

Estimating BP using PAT became popular because it is easy to obtain by referencing the ECG R wave, which is precise and easy to get. The disadvantage is the introduction of the PEP variable, especially when PTT is small and the distal measurement point is close to the core body. Although some studies have claimed that PAT is a better indicator of SBP due to its dependency on both ventricular contraction and vascular function, it is generally thought that PTT has higher correlation with SBP, DBP, and MAP than PAT [17].

3.6 Pulse Wave Analysis

Pulse Wave Analysis (PWA), is a technique which consists of the morphological analysis of the pressure pulse waveform. Its shape reflects information about the properties of the arterial wall and the state of ventricular ejection [17]. Several PWA features have been linked to indicators of cardiovascular health and diseases in many clinical studies.

In addition, this technique and can provide an indirect means of assessing blood pressure itself by means of the PPG waveform. It has been shown that the PPG signal at the fingertip is influenced by the same physiological determinants as the radial pressure waveform and undergoes similar morphological changes in vascular disease [17]. It's not possible to directly extract blood pressure information from the PPG waveform since its amplitude is related to tissue perfusion. However, the morphology of the PPG, which is similar to the one of the pressure waveform, contains relevant features for blood pressure estimation. These features can be translated into blood pressure values if an adequate calibration procedure, also caled "initialization" [17] is performed.

Some of pulse wave analysis features which can be extracted from the PPG have been inspired in features commonly used to analyse blood pressure pulse waveforms, such as the augmentation index, the diastolic time (time at which systolic blood pressure reaches its peak) and the time to systolic peak [17]. However, the PPG waveform contains some differences from the pressure pulse and therefore many PPG-specific features have been proposed in the literature for the analysis of PPG waveforms, namelly:

- Systolic amplitude: peak-to-peak amplitude of the PPG wave
- Reflection index: $RI = y/x$, where y is the height of the diastolic peak and y is the height of the systolic peak
- Index of the stiffness of the large arteries: $SI = h/\Delta T$, where h is the height of the subject and ΔT is the time delay between the systolic and diastolic peaks

Several features can also be derived from the second derivative of the PPG (sdPPG), or acceleration plethysmogram (APG). The sdPPG signals is characterized by several peaks and valleys respectively designated as a-wave (early systolic positive wave), b-wave (early systolic negative wave), c-wave (late systolic reincreasing wave), d-wave (late systolic redecreasing wave) and e-wave (early diastolic positive wave) [5].

4

State of the art on cuffless BP estimation

This chapter presents current state of the art in the field of continuous cuffless blood pressure estimation. This includes both methods based on physiological models and data-driven methods, using machine learning techniques. The most relevant literature methods found are discussed in detail.

4.1 Introduction

Cuffless blood pressure estimation has been extensively studied over the last years. The classical BP estimation models consist of mapping indicators that can reveal the BP changes, such as PTT, PAT and others defined in the previous section, to the BP values [17]. Several approaches have been attempted to model the relationship between BP indicator variables and BP and they can be roughly divided in two groups. One of the possible approaches consists of using theory-based mathematical models to map the relationship between these indicators and the BP, requiring expert knowledge of the underlying

physiologically processes. The alternative are data-driven approaches, based on machine learning techniques.

4.2 Model-Based Methods

Early studies such as those by Chen et al. and Poon et al., two of the most cited works in the field, developed PTT models for BP estimation based on the Moens-Korteweg equation, which correlates PWV with the modulus of elasticity of the arterial wall [17].Although their results demonstrated that PTT is able to track BP, both models have shortcomings such as limited accuracy and short calibration intervals [28]. More recently in 2015, PIR (the photoplethysmogram intensity ratio) was proposed as a new indicator for BP estimation in a study by Ding et al [29]. The inclusion of this parameter, which can be affected by changes in the arterial diameter, improved the estimation when compared to BP models based only on PTT.

The theory-driven model-based methods have the advantages of being generalizable and interpretable. However, the relationship between BP indicators has been demonstrated to be more complicated than a simple linear or nonlinear regression model. In the case of PTT, it has been shown to have distinct correlation with BP among different individuals [17]. There are many factors affecting blood pressure, such as age, temperature, mental stress, and different behaviour pattern, which are not reflected in this indicator.

4.3 Data-driven Methods

Machine learning methods are particularly valuable for cuffless BP estimation due to their ability to constantly learn from data. Also, machine learning techniques allow the use of multiple indicators for the estimation, which would be difficult to integrate in a physiological mathematical model, and may prevent BP prediction from being affected by confounding factors or noise in a single indicator [30].

One of the first to study this approach was Monte-Moreno, who combined a set of features describing several PPG characteristics in several machine learning techniques to predict continuous SBP [30]. Ridge linear regression, a multilayer perceptron neural network, support vector machines and random forests where tested, and the best performance was obtained with the Random Forest Tree method, which has resulted in a coefficient of determination between the reference and the prediction of 0.91 and 0.89 for SBP and DBP, respectively [17].

Later, in a study by Ruiz-Rodriguez [31], a neural network based method based on PPG features was studied on patients undergoing continuous invasive BP measurement with an arterial catheter. The validation group included 47 patients and the results obtained were not satisfactory to allow clinical

application [31].

In 2013, Kurylyak et al. also used an Artificial Neural Network (ANN) and a set of 21 features extracted from the PPG waveform to estimate SBP and DBP. Training and test data were extracted from the MIMIC database and the estimation results presented a MAE of $3.80 \pm 3.46 mmHg$ SBP and $2.21 \pm 2.09 mmHg$ for DBP. However, no information is given on the amount of subjects in which it was tested [32].

With recent developments in machine learning, more advanced methods such as Deep Neural Networks have also been used to model the nonlinear relationship between the BP predictors and BP measurements. Temporal dependencies between the raw input signals and blood pressure pressure have also been model using recurrent neural networks [17].

4.4 State of the art research

4.4.1 Search strategy

Although cuffless and continuous blood pressure has been studied in the past, this systems do not yet comply with the standards required to be applied in clinical practise, so there is currently a great interest in developing such systems. In fact, a lot of recent studies have developed methods for BP estimation. However, the application required for this project, namely applying the BP estimation method to the data acquired in the WARD project, limits the amount of studies that are considered relevant. The main search goal was therefore to find cuffless blood pressure estimation methods that could be integrated in the WARD system.

The literature research was performed using two search engines: *findit.dtu.dk* and *Google Scholar*. Several combinations of keywords were used for free word search. The words used are: cuffless, continuous, blood pressure, estimation, photopletysmogram, PPG. The search resulted in thousands of results so an inclusion criteria was defined based on the publication year. The inclusion criteria defined were:

- Publication year: 2016 - present
- Online access available

Other exclusion criteria were defined based on the specific characteristics of the data available. Studies with the following characteristics were excluded:

- specific hardware built for the purpose of the study
- measurements requiring procedures to induce BP changes for calibration (Valsalva manoeuvre, cold pressure test or others)

- unspecified BP estimation methodology
- only classification of BP in ranges of values (normotension, hypertention and pre-hypertension for instance)

4.4.2 Selected Studies

After the research procedure described in the previous section the studies which achieved more promising results were selected and will next be reviewed in detail. In most studies, the results are evaluated using the Association for the Advancement of Medical Instrumentation (AAMI) Standard, which requires BP measurement devices to have Mean Error (ME) and Standard Deviation (STD) values lower than 5 and 8 mmHg, respectively [33]. It additionally requires devices to be evaluated on a statistical population of at least 85 subjects, as shown in table 4.1. Some studies are also evaluated according to the the British Hypertension Society (BHS) Standard [34], which grades BP measurement devices based on their cumulative percentage of errors, as specified in table 4.2.

In table 4.3, a summary of the most relevant studies in the field is presented.

Table 4.1: Comparison with the AAMI standard

	ME (mmHg)	STD (mmHg)	Subjects
SBP and DBP	≤ 5	≤ 8	≥ 85

Table 4.2: Comparison with the BHS standard

	Cumulative Error Percentage		
	$\leq 5mmHg$	$\leq 10mmHg$	$\leq 15mmHg$
grade A	60%	85%	95%
grade B	50%	75%	90%
grade C	40%	65%	85%

(Kachuee2017) Cuffless Blood Pressure Estimation Algorithms for Continuous Health-Care Monitoring [7]

Purpose: To develop an algorithm, based on PAT features, heart rate (HR), Augmentation Index (AI), Large Artery Stiffness Index (LASI) and Inflection Point Area Ratio (IPA) for the continuous (in an order of seconds) and cuffless estimation of the systolic blood pressure, diastolic blood pressure, and mean arterial pressure values.

Methods: The proposed framework estimates the BP values based on ECG and PPG signals and was tested on data available in the MIMIC II online waveform database. The signals are first processed to remove the effects of noise and artifacts from the raw signals using discrete wavelet decomposition.

Next, two types of features can be extracted, which are based on either physiological parameters or whole-based representation of vital signals. Several machine learning algorithms are then tested for the regression task, namely Regularized Linear Regression, Decision Tree Regression, Support Vector Machine (SVM), Adaptive Boosting (AdaBoost) and Random Forest Regression (RFR). Separate models are trained for the estimation of the SBP, DBP, and MAP, even though the same feature vectors are used. Finally, there is an optional calibration procedure, which can improve the system's accuracy.

Results: The parameter-based feature extraction approach slightly outperformed the whole-based method and the AdaBoost approach performed better that the others regarding mean absolute error (MAE). It was also observed that the calibration-based approach outperformed the calibration-free approach with a considerable margin. The proposed method was also evaluated using the Association for the Advancement of Medical Instrumentation and the British Hypertension Society standards. For comparison with the AAMI standard the RFR learning method was used, since it presents results with lower STD values, which is an important criterion of the AAMI standard. The results comply with the AAMI standard in the estimation of DBP and MAP and regarding the BHS protocol the results achieve grade A for the estimation of DBP and grade B for the estimation of MAP.

Conclusion: By using PAT in combination with other feature from the ECG and PPG signal it is possible to obtain a reliable estimation of BP, and the BP estimation algorithm shows satisfactory results even when no calibration procedures are used

Comments: Although the results do not meet the AAMI standard for SBP estimation (in terms of SD), the method was tested on 942 subjects, when the standard only requires evaluation in at least 85. Also, the MIMIC database contains only data from patients in intensive care units (ICU), potentially having abnormal BP variations. Therefore, a more diverse population including also healthy and younger subjects would likely lead to improved results.

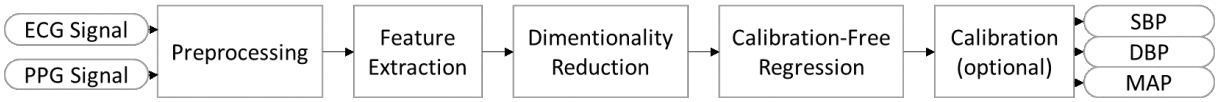

Figure 4.1: Block diagram of the cuffless BP estimation method proposed by Kachuee et al.

(Ding2017) Pulse Transit Time Based Continuous Cuffless Blood Pressure Estimation: A New Extension and A Comprehensive Evaluation [22]

Purpose: The purpose of this work is to extend the PTT based cuffless BP measurement method by introducing a new indicator – the photoplethysmogram intensity ratio (PIR) and to give insights into

cuffless BP measurement for tracking dynamic BP changes and over extended calibration intervals.

Methods: A new model that relates PTT and PIR with DBP and SBP is proposed. PIR is extracted from the PPG waveform, whereas PTT is extracted from ECG and PPG. The performance of two PTT and PIR models and 6 models based only on PTT was compared. The validation was conducted on 33 subjects with and without hypertension, at rest and under various maneuvers with induced BP changes (namely deep breathing, Valsalva manoeuvre and sustained handgrip). For each of the tests either one or two heartbeat periods were used for calibration. The measurement at rest was also performed on 8 subjects one day after the first measurement, without repeating the calibration procedure.

Results: The proposed methods achieved better accuracy on each subject group at rest state and over 24 hours calibration interval, comparing to the PTT models. Among all, the proposed method PTT&PIR#2 performed the best, with estimation errors for SBP and DBP being $1.17 \pm 5.72 mmHg$ and $0.40 \pm 7.11 mmHg$, respectively. The BP estimation errors under dynamic maneuvers, over extended calibration interval were significantly higher for all methods. Regarding the extended calibration interval, PTT&PIR#2 method performed better compared to the others.

Conclusion: The PIR shows potential as an additional indicator for improving the accuracy of cuffless BP measurement.

Comments: This model still requires conduction of a conventional BP measurement to perform calibration of the model for each subject, and it was not tested on enough subjects in order to meet the AAMI standards. Also, since calibration was performed before each of the dynamical experiments, it is not possible to confirm the robustness of the method.

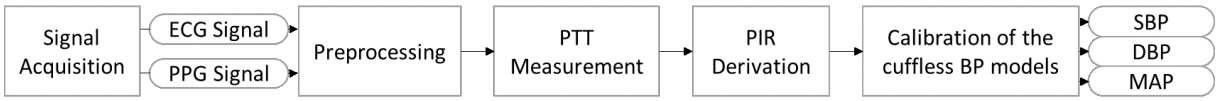

Figure 4.2: Block diagram of the cuffless BP estimation method proposed by Ding et al.

(Miao2017) A Novel Continuous Blood Pressure Estimation Approach Based on Data Mining Techniques [8]

Purpose: To propose a novel continuous BP estimation approach that combines data mining techniques, namely two multivariate analysis methods, with a traditional mechanism-driven model. Also aims at validating the proposed method over different time intervals and in both static and dynamic conditions.

Methods: First, 14 features derived from simultaneous electrocardiogram and photoplethysmogram signals were extracted for beat-to-beat BP estimation. A genetic algorithm-based feature selection method was then used to select the 10 most critical features for each subject. Multivariate linear regression (MLR) and support vector regression (SVR), were adopted to develop the BP model based on the features selected by the genetic algorithm. The model was validated with a static BP estimation experiment on 73 healthy adults, a dynamic experiment on 35 subjects (after 5 min of rope skipping) and follow-up experiments on 10 subjects. Follow-up validation experiments were conducted 1 day, 3 days and 6 months after the first experiment.

Results: In static BP estimation, the approach showed a correlation coefficient and mean error of 0.852 and $-0.001 \pm 3.102 mmHg$ for systolic BP, and 0.790 and $-0.004 \pm 2.199 mmHg$ for diastolic BP. Similar performance was observed for dynamic BP estimation. The estimation error increased from -0.001 ± 3.102 to $0.85 \pm 5.78 mmHg$ for SBP and from -0.004 ± 2.199 to $-1.24 \pm 4.63 mmHg$ for DBP at 1 day after the initial calibration. However, it was relatively stable from 1 day to 3 days and to 6 months after construction of the model.

Conclusion: This approached showed improved accuracy when compared to a PTT+PIR method.

Comments: This approach is patient-specific since the BP estimation model must be constructed for each subject, which improves the results when compared to other methodologies. However, this makes it less suitable to implement in clinical settings.

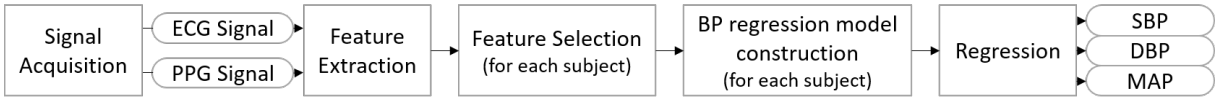

Figure 4.3: Block diagram of the cuffless BP estimation method proposed by Miao et al.

(Xing 2019) An Unobtrusive and Calibration-free Blood Pressure Estimation Method using Photoplethysmography and Biometrics [4]

Purpose: To develop a method to unobtrusively and optically measure blood pressure without calibration and study it on subjects with diverse biometrics.

Methods: PPT was estimated based only on an index of large artery stiffness which requires only PPG signal and height information. Whole based features were extracted from the PPG and the sdPPG waveform. Values of b/a, c/a, d/a and e/a, in which a, b, c, d and e are the amplitudes of the respective waves in the sdPPG waveform. In total, 19 features were used as input to a random forest algorithm.

The model was tested on 1248 subjects with various age, height, weight and BP levels, and PPG measurements were performed for 60 seconds. A calibration procedure was also tested on a group of 147 subjects.

Results: BP estimation accuracy was tested separately for different subgroups: younger and older populations; groups with low peripheral perfusion index and high peripheral perfusion index and groups with different degrees of hypertension. Using the model without calibration the fitting errors in the young population (<50 years old) with low, medium and high SBP (120mmHg, 120-139mmHg and $\geq$ 140mmHg, respectively) were 6.3 ± 7.2, -3.9 ± 7.2 and -20.2 ± 14.2 mmHg for SBP respectively. In the older population (>50 years old) the fitting errors with low, medium and high SBP were 12.8 ± 9.0, 0.5 ± 8.2 and -14.6 ± 11.5 mmHg for SBP respectively. The results were significantly improved when calibration was used.

Conclusion: PPG may be used to calculate BP without calibration in certain populations, namely those with good peripheral perfusion, the normotensive and the pre-hypertensive. However with personalized calibration PPG-based BP estimation accuracy is significantly improved.

Comments: This approach is particularly interesting given that it is based only on the PPG signal. Although the results do not meet the AAMI standards, the method has been tested on a very wide population.

Figure 4.4: Block diagram of the cuffless BP estimation method proposed by Xing et al.

(Mousavi 2018) Blood pressure estimation from appropriate and inappropriate PPG signals using a whole-based method [35]

Purpose: To propose an algorithm for noninvasively, cuff-less and calibration-free BP estimation, using only the PPG signal regardless of its shape (appropriate or inappropriate).

Methods: The method proposed is evaluated on PPG and ABP data from the MIMIC II database belonging to 441 subjects. For each subject, three 15 seconds records are considered, resulting in a total of 1323 records. The PPG signals are first pre-processed using a Fast Fourier Transform (FFT) filter. The proposed whole-based method then considers all values of the PPG signal at a specific distance between two consecutive R peaks in an ECG signal as the feature vector. The length of the

feature vectors is then reduced by using the principal component analysis (PCA) algorithm. Each of these vectors is then used an input of the machine learning algorithms applied, namely Decision tree regression, Support vector regression (SVR), Adaptive Boosting (AdaBoost) regression and Random Forest Regression (RFR). Train and test data are separated by a 10-fold cross validation procedure.

Results: The best results were obtained with Adaptive Boosting, with estimation errors of $0.187 \pm 4.173 mmHg$, $0.067 \pm 4.911 mmHg$ and $-0.050 \pm 8.901 mmHg$ for DBP, MAP and SBP respectively. The results are met by the AAMI standard for both MAP and DBP estimations but not for SBP estimation. According to the BHS standard, the proposed algorithm for DBP estimation got grade A, whereas it got grade B for estimation of MAP and got approximately grade C for SBP estimation.

Comments: The results seem to indicate that the proposed algorithm can be used for BP estimation. However, the fact that measurements from the same subject can be present in both the training and test set set may lead to over optimistic results, as it mimics a calibration procedure.

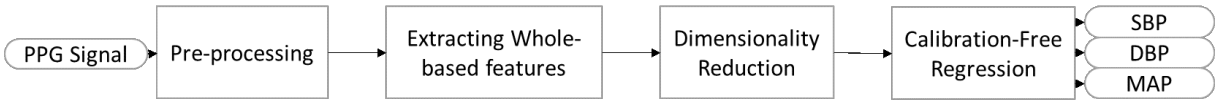

Figure 4.5: Block diagram of the cuffless BP estimation method proposed by Mousavi et al.

(Wang 2018) A Novel Neural Network Model for Blood Pressure Estimation Using Photoplethesmography without Electrocardiogram [36]

Purpose: To develop a method for estimating systolic and diastolic BP based only on a PPG signal, using a multitaper method to obtain the spectral components of a PPG signal and combining them with two morphological features of the PPG.

Methods: To train and test the proposed model, data was extracted from the MIMIC database. Namelly, 58,795 valid intervals of PPG signal (subject number is 72) and corresponding BP values for different people and different time instances were used (70% of them for network training, 15% of them for validation, and 15% of them for testing). Spectral features were extracted from the PPG signals using the multitaper method and two morphological features (systolic upstroke time (ST) and diastolic time (DT)) were also extracted. This resulted in a total of 22 parameters being used to are used to train the Artificial Neural Network (ANN), which was performed using the Levenberg-Marquardt algorithm.

Results: The proposed method resulted in mean absolute error of $4.02 \pm 2.79 mmHg$ for systolic BP and $2.27 \pm 1.82 mmHg$ for diastolic BP.

Comments: The results meet the AAMI criteria regarding mean error and standard deviation. However, the algorithm was not tested in a sufficient number of subjects.

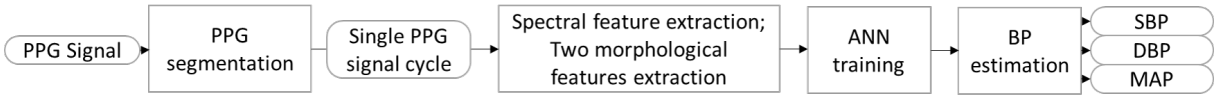

Figure 4.6: Block diagram of the cuffless BP estimation method proposed by Wang et al.

(Thambiraj2019) Noninvasive cuffless blood pressure estimation using pulse transit time, Womersley number, and photoplethysmogram intensity ratio [37]

Purpose: To develop a novel BP algorithm based on the Morgan and Kiley expression and using PTT, PIR (which can echo the change in vasomotor tone), and the Womersley number (α), which reflects the fluid flow with respect to viscous effects of the blood, for the improvement of accuracy in BP estimation.

Methods: The algorithm was evaluated with 42 healthy and 39 diseased subjects and two trials were performed for each subject. In each trial ECG and PPG signals were recorded for 3 min in a seated rest position and the PTT, PIR and alpha parameter were obtained as an average of the first 30 s of the recording. The alpha parameter is derived from the values of blood viscosity, which in turn are found from the PPG signal (considered a surrogate for the blood viscosity measurement). Pulse pressure (PP) was then derived from PIR, PTT and the alpha parameter, and MAP, SBP and DBP were estimated using the proposed model.

Results: Errors of 0.13 ± 2.12, -0.10 ± 1.20, -0.013 ± 1.08 were obtained in the estimation of SBP, DBP and MBP of healthy subjects' and in diseased subjects the errors obtained were 0.23 ± 2.30, -0.24 ± 1.50, -0.047 ± 0.070 for SBP, DBP and MAP, respectively.

Comment: Although the results meet the AAMI criteria, the reference blood pressure measurements are not performed with a continuous noninvasive blood pressure system, but with a cuff-based device, and one-to-one calibration is required.

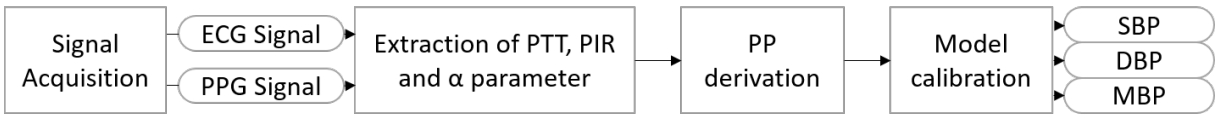

Figure 4.7: Block diagram of the cuffless BP estimation method proposed by Thambiraj et al.

(Su2018) Long-term Blood Pressure Prediction with Deep Recurrent Neural Networks [38]

Purpose: To propose a new method for arterial blood pressure estimation, focusing particularly on proving the importance of modelling temporal dependencies in BP dynamics for accurate BP prediction. To improve the accuracy of multi-day BP prediction, BP estimation is formulated as a sequence prediction problem in which both the input and target are temporal sequences.

Methods: The architecture of the deep recurrent neural network (RNN) proposed as BP estimation model is first defined. It consists of a bidirectional Long Short-Term Memory (LSTM) at the bottom layer, and a stack of multi-layered LSTM with residual connections. The bidirectional structure was designed to access larger-scale context information of input sequence. The residual connections allow gradients in deep RNN to propagate more effectively. RNN models with 2, 3 and 4 layers were then evaluated on both a static and multi-day continuous BP dataset. The input features correspond to handcrafted features of ECG and PPG signals (PTTs, Heart rate, Reflection Index, Systolic Timespan, Up Time, Systolic Volume and Diastolic Volume). Each training dataset was divided such that 70 % of the data was used for training, 10 % for validation and 20 % for test. Finally, a comparison of the model proposed with two pulse transit time models, support vector regression (SVR), decision tree, and Bayesian linear regression models and Kalman filter model was performed.

Results: On the static continuous BP dataset, the best accuracy was obtained by the proposed 4-layer deep RNN (DeepRNN-4L) model which achieves a RMSE of 3.73 and 2.43 for SBP and DBP prediction respectively. On a multi-day BP dataset, the deep RNN achieved RMSE of 3.84, 5.25, 5.80 and 5.81 mmHg for the 1st day, 2nd day, 4th day and 6th month after the 1st day SBP prediction, and 1.80, 4.78, 5.0, 5.21 mmHg for corresponding DBP prediction.

Comments: Since the the mean error and standard deviation were not computed, it is not straightforward to compare the performance with other studies and the AAMI standard.

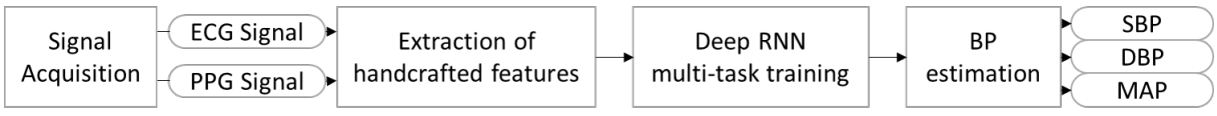

Figure 4.8: Block diagram of the cuffless BP estimation method proposed by Su et al.

Table 4.3: Summary of the recent studies proposing methods for cuffless BP estimation. (* - studies found more relevant and which have been described in detail in the previous sections)

Author (Year)	Modalities	Features	Model/ Method	Dataset	BP Reference	Patient-specific Calibration	Lowest estimation errors (mean±SD) [mmHg]
Kachuee et al. (2017)* [7]	ECG, PPG	(1) PAT features, HR, AI, LASI, IPA; (2) Whole-Based Features	Regularized Linear Regression; Decision Tree Regression; SVM; AdaBoost; RFR	942 subjects (MIMIC II database)	ABP	Optional	SBP: -0.06 ± 9.88 MBP: 0.16±5.25 DBP: 0.36±5.70 (No calibration)
Ding et al. (2017)* [22]	ECG, PPG	PTT, PIR	$SBP = MBP_0 \cdot \frac{PIR_0}{PIR} + \frac{2}{3} \cdot \frac{PIR}{PIR_0} \cdot \left(\frac{PTT_0}{PTT}\right)^2$ $DBP = MBP_0 \cdot \frac{PIR_0}{PIR} - \frac{1}{3} \cdot \frac{PIR}{PIR_0} \cdot \left(\frac{PTT_0}{PTT}\right)^2$	14 hypertensive and 19 healthy subjects;	Finapres	Yes	SBP: 1.17±5.72 DBP: 0.40±7.11
Miao et al. (2017)* [8]	ECG, PPG	14 ECG/PPG features	MLR; SVR	73 healthy subjects + 35 subjects (dynamic experiment) + 10 subjects (long-term experiment)	Finapres	Yes	SBP: -0.001 ± 3.102 DBP: -0.004 ± 2.199
Xing et al. (2019)* [4]	PPG	19 SDPTG-based and whole based features	RFR	1249 subjects + 147 subjects for calibration tests	electronic sphygmo-manometer	Optional	Young group: SBP: 0.45 ± 11.3 DBP: 0.31 ± 8.55 Older group: SBP: -0.68 ± 14.1 DBP: 0.20 ± 9.0 (No calibration)
Ding et al. (2017)* [22]	ECG, PPG	PTT, PIR	$SBP = DBP_0 \cdot \frac{PIR_0}{PIR} + PP_0 \cdot \frac{PIR}{PIR_0} \cdot \left(\frac{PTT_0}{PTT}\right)^2$ $DBP = DBP_0 \cdot \frac{PIR_0}{PIR} +$	27 healthy subjects	Finapres	Yes	SBP: 0.37 ± 5.21 DBP: - 0.08 ± 4.06 MBP: - 0.18 ± 4.13
Mousavi et al. (2018) [35]*	PPG	PPG whole based features	AdaBoost regression	441 subjects (MIMIC II database)	ABP	No	SBP: -0.05 ± 8.90 MBP: 0.07 ± 4.91 DBP: 0.19 ± 4.17

Wang et al. (2018)* [36]	PPG	PPG Spectral and Morphological features	ANN (one hidden layer)	72 subjects (MIMIC database)	ABP	No	SBP: 4.02 $\pm$ 2.79 DBP: 2.27 $\pm$ 1.82
Thambiraj et al. (2019)* [37]	ECG, PPG	PTT, PIR, α		42 healthy subjects; 39 diseased subjects	Omron BP monitor	Yes	Healthy: SBP: 0.13 $\pm$ 2.12, DBP: -0.10 $\pm$ 1.20 MBP: -0.013 $\pm$ 1.08 Diseased: SBP: 0.23 $\pm$ 2.30 DBP: -0.24 $\pm$ 1.50 MBP: -0.047 $\pm$ 0.070
Su et al. (2018)* [38]	ECG, PPG	7 ECG/PPG features	Four-layer deep RNN (LSTM)	84 healthy subjects + 12 healthy subjects for multi-day experiments	Finapres	No	SBP: 3.73 mmHg (RMSE) DBP: 2.43 mmHg (RMSE)
Tanveer et al. (2019) [39]	ECG, PPG	PTT and morphological features from ECG and PPG	Waveform based hierarchical Artificial Neural Network–Long Short Term Memory (ANN-LSTM) model	39 subjects (MIMIC I database)	ABP	Yes	SBP: 0.0159 $\pm$ 1.2630 DBP: 0.0018 $\pm$ 0.7280
Lin et al. (2018) [40]	ECG, PPG	(1) 19 PPG indicators and PTT (2) 19 PPG indicators	linear regression algorithm	22 healthy subjects	Finapres	Yes	SBP: 2.75 $\pm$ 7.34 DBP: 2.71 $\pm$ 4.72 With (PPG + PTT)-based method
Xing et al. (2016) [41]	PPG	Spectrum amplitude and phase of PPG	ANN with one hidden layer	69 patients (MIMIC II database)	Omron HEM-7051 BP monitor	No	SBP: 0.06 $\pm$ 7.08 DBP: 0.01 $\pm$ 4.66

Sharifi et al. (2019) [42]	ECG, PPG	PTT and PIR	regression by use of MARS method	MIMIC II database (3663 records)	ABP	Yes	DBP: -0.09 $\pm$ 5.21 MBP: -0.16 $\pm$ 4.6 SBP: -0.29 $\pm$ 9.1
Chen et al. (2018) [43]	ECG, PPG	heart-rate power spectrum ratio (HPSR), PTT and PIR	$SBP = (SBP_0 - DBP_0) \cdot \left(\frac{PTT_0}{PTT}\right)^2 + DBP_0 \cdot \frac{ln\, PIR_0}{HPSR_0} \cdot \frac{ln\, PIR}{HPSR} + PIR + PTTV$ $DBP = DBP_0 \cdot \frac{ln\, PIR_0}{HPSR_0} \cdot \frac{ln\, PIR}{HPSR} + PIRV$	60 subjects (29 hypertensive and 31 normotensive)	mercury sphygmo-manometer	Yes	Hypertensive: SBP: 0.73 $\pm$ 10.04 DBP: 0.90 $\pm$ 7.10 Normotensive: SBP: 0.54 $\pm$ 7.52 DBP: 0.82 $\pm$ 6.20
Lin et al. (2017) [44]	PPG, ECG	PTT and 1st dPIR	$SBP = a \cdot PTT + b \cdot \frac{1}{1^{st}dPIR} + c$ $DBP = d \cdot PTT + e \cdot \frac{1}{1^{st}dPIR} + f$	22 healthy subjects	Finapres	Yes	SBP: 3.22 $\pm$ 8.02 DBP: 3.13 $\pm$ 4.82
Khalid et al. (2018) [45]	PPG	pulse area, pulse rising time and width 25%	regression tree, MLR and SVM	32 cases from the University of Queensland vital sign dataset	noninvasive blood pressure	—	SBP: -0.1$\pm$6.5 DBP: -0.6$\pm$5.2
Radha et al. (2018) [30]	PPG, accele-rometer	Activity features, Heart rate variability, PPG morphology features	sequence-to-sequence model: perceptron + LSTM	120 subjects	ambulatory BP monitor	Yes	SBP: 5.65 mmHg (RMSE)

5

Blood Pressure Estimation Methods

This chapter describes the methods used in development of the blood pressure estimation algorithm. This includes data description and selection, signal processing, feature extraction and regression algorithm. The blood pressure estimation method developed, inspired by the literature studies described in the previous section, was first applied to the MIMIC II database data. On a second step, this method was adapted to be applied to the WARD data.

5.1 MIMIC Database

5.1.1 Dataset

The data used are from the Multi-Parameter Intelligent Monitoring for Intensive Care II (MIMIC II) database. MIMIC II is a freely available database that contains data from more than 25000 ICU patients who stayed in critical care units of the Beth Israel Deaconess Medical Center in Boston, Massachusetts. Data were collected over a seven year period, beginning in 2001 [46]. The database contains two types of data, namely, clinical data stored in a relational database and waveform data recorded by the bed-

side monitors. The clinical database contains diverse information, such as hourly measurements of vital signs, lab test results, medical procedures, medications, mortality information, among others. The waveform data (MIMIC-II Waveform Database) contains records from a subset of patients and includes physiological signals such as electrocardiogram (ECG), photopletysmogram (PPG) and intra-arterial blood pressure (ABP). Only part of the waveform data have been matched to the clinical data in the relational database [46].

The particular version of the database used (MIMIC II Waveform Database Matched Subset, version 3.1, which can be found at https://archive.physionet.org/physiobank/database/ mimic2wdb/matched/) contains 4,897 waveform records and 5,266 numerics records matched with 2,809 MIMIC II Clinical Database records. Not all signals are available for all of the subjects in this subset. Therefore, records containing simultaneous PPG, ABP and ECG lead II waveforms with minimum durations of 10 minutes were selected.

Since the data represent realistic ICU measurements, noise, missing data gaps and artifacts are commonly encountered, due to patient movement, sensor degradation, transmission errors, electromagnetic interference and human error [46]. Liang et al. [6] have analysed ABP, ECG and PPG records from the MIMIC II database and identified abnormal (low quality) signals, as shown in figure 5.1, which were excluded from the present analysis. However, since in this work a more recent version of the database, containing more records, was used, there are still abnormal signals present in the analysed subset, which for the most part should be excluded by the pre-processing steps. The records selected are from a total of 146 patients and have durations from 10 minutes to 1 hour. The distribution of systolic and diastolic blood pressure records is shown in figure 5.2.

The authors of the database also mention the possibility of errors in the data matching and alignment. In particular, the waveform data may contain unknown inter-channel delays, which may not be constant in a given record [46]. This makes the extraction of pulse transit times unreliable in most cases, which has also been demonstrated by Liang et al [6].

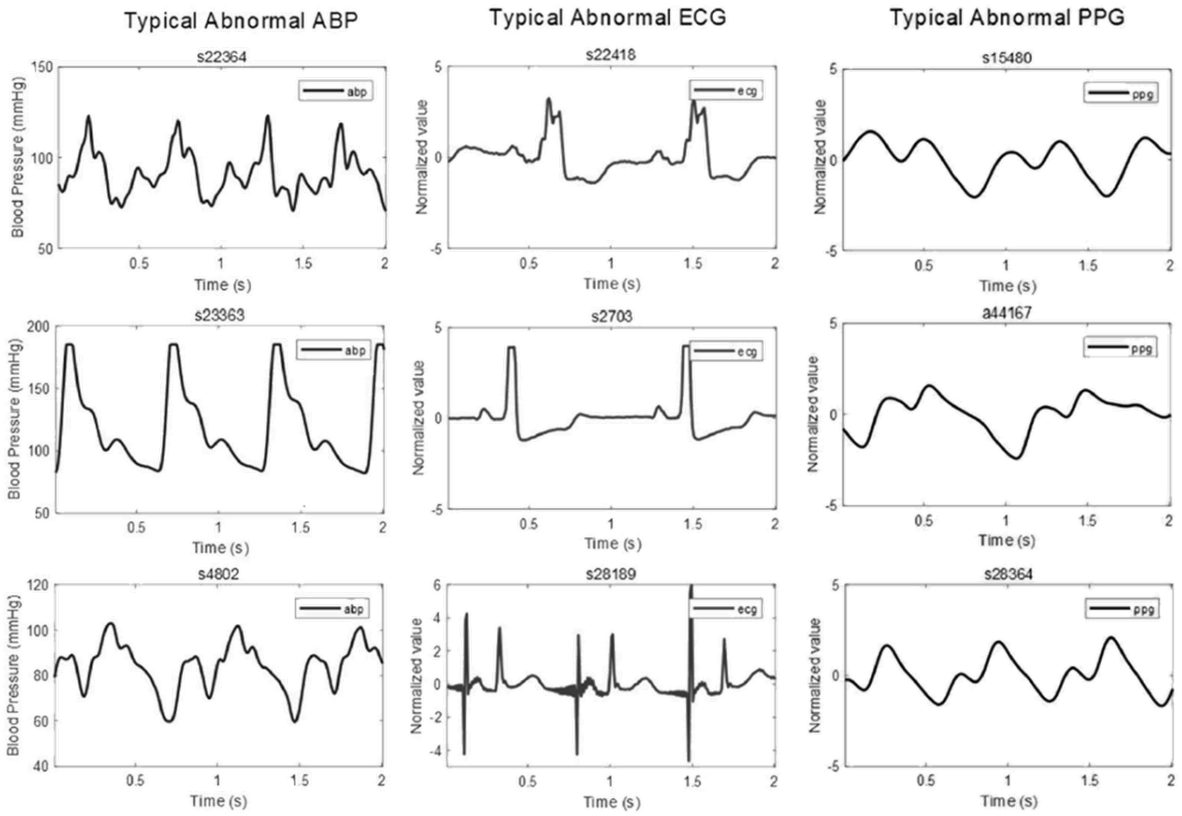

Figure 5.1: Typical cases of abnormal waveforms. An "abnormal" ABP signal refers to an ABP signal where the systolic and diastolic waves cannot be distinguished, or their morphologies are highly distorted; An "abnormal" ECG signal refers to an ECG signal where the morphology of the QRS waves is highly distorted; An "abnormal" PPG signal refers to a PPG signal where the systolic and diastolic waves cannot be distinguished, their morphologies are highly distorted, and heart rate cannot be determined. Adapted from [6]

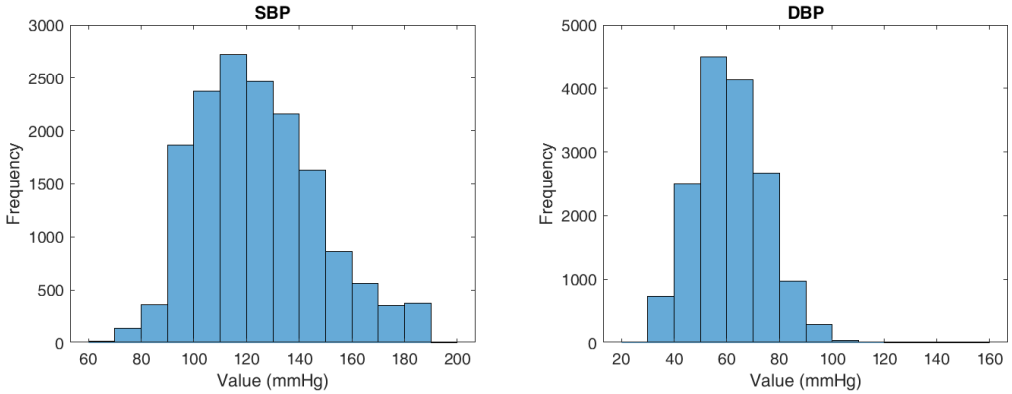

Figure 5.2: Distribution of parameters in the records selected from the MIMIC II database: systolic blood pressure (SBP) and diastolic blood pressure (DBP)

The steps implemented to estimate blood pressure from the data extracted from the MIMIC II database are described in figure 5.3, and will be described in detail in the following sections.

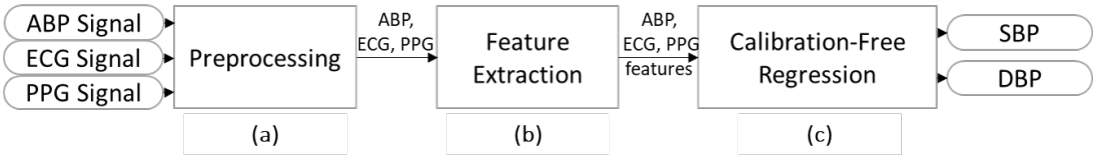

Figure 5.3: Block diagram of the proposed cuffless BP estimation method, where SBP and DBP features used as label are extracted from the ABP signal. The steps in blocks (a), (b) and (c) are described in sections 5.1.3, 5.1.4 and 5.3, respectively.

5.1.2 State of the art method implementation

To establish a basis for comparison, the method by Kachuee et al. [7] described in the previous chapter was implemented. This method was selected based on performance results, number of subjects in which they were evaluated and the absence of calibration. This paper suggests two different implementations, as mentioned in section 4.4.2. In the first, features extracted from the PPG and ECG signals are based on physiological parameters. On the alternative, a whole-based representation of vital signals is used. The first was chosen since it yielded better BP estimation results. The model was trained and tested on the MIMIC II data described in the previous section. The Random Forest Regression was the algorithm selected, as it led to the best estimation results in the paper, and feature vector used as input contained the features described in figure 5.7 and table 5.2.

5.1.3 Pre-processing

The ABP, PPG and ECG signals are first resampled from 125 Hz to 1000Hz using linear interpolation, as illustrated in figure 5.4. The PPG and ECG signals are then filtered and denoised using discrete wavelet transform (DWT), following a similar method to [7]. The signal is decomposed to level 10 using DWT with the Daubechies 8 (db8) mother wavelet. Both low frequencies (from 0 to 0.98Hz) and high frequencies (from 250 to 500 Hz) are removed by zeroing the respective decomposition coefficients, illustrated in figure 5.5. Wavelet denoising is then performed on the remaining coefficients using *MATLAB* function `wdenoise`, which consists of three main steps [47]:

- Decomposition — Compute the wavelet decomposition of the signal at level 10.
- Detail coefficients thresholding — For each level from 1 to 10, select a threshold and apply soft thresholding to the detail coefficients. The threshold selection rule is based on Stein's Unbiased Estimate of Risk (SURE), a quadratic loss function. After an estimate of risk is obtained for a particular threshold value, t, the algorithm then minimizes the risks in t to yield a threshold value [47].

- Reconstruction — Compute wavelet reconstruction based on the original approximation coefficients of level 10 and the modified detail coefficients of levels from 1 to 10.

An example of the filtering process result is illustrated in figure 5.6

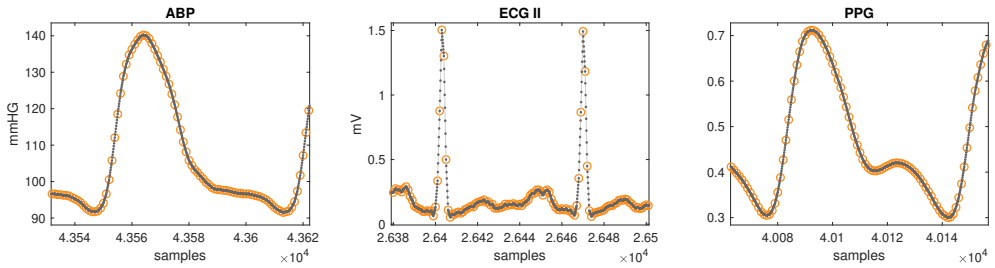

Figure 5.4: Example of the result of the resampling process of the ABP, ECG and PPG signals. The original data points, sampled at a 125Hz frequency, are plotted in orange and the resulting points, sampled at a 1000Hz frequency, in grey.

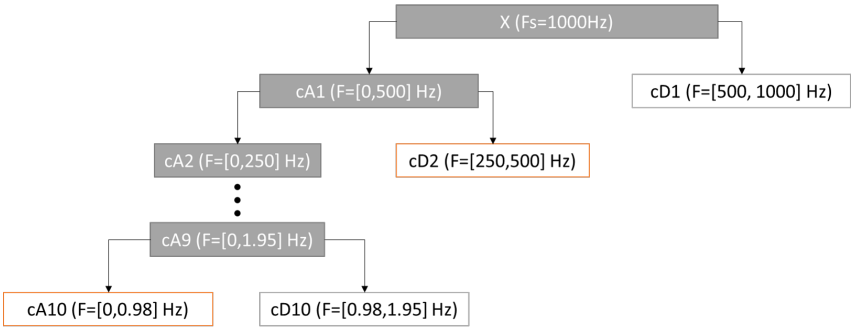

Figure 5.5: Wavelet decomposition structure of the PPG and ECG signals. X represents the data array being pre-processed, cD*i* are the level *i* detail coefficients and cA*i* are the level *i* approximation coefficients. The coefficients and corresponding frequencies highlighted in orange are the ones being removed by the pre-processing algorithm

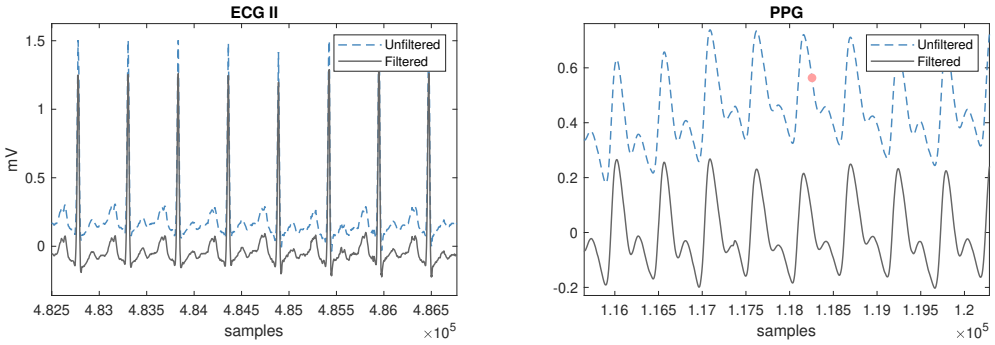

Figure 5.6: Example of the result of the filtering process in the ECG (left) and PPG (right) signals. The original signals are plotted in blue and the filtered signals in grey.

BP signal cleaning

Systolic blood pressure (SBP) and diastolic blood pressure (DBP) are computed for each heart cycle. Abnormal SBP and DBP values are discarded, using a method based on the signal abnormality index (SAI) proposed by Sun et al [11]. The BP data exclusion criteria are shown in table 5.1. The mean arterial pressure (MAP) is defined as:

$$MAP = \frac{2DBP + SBP}{3} \tag{5.1}$$

Table 5.1: Features computed from the ABP signal and respective abnormality criteria. Adapted from Sun et al. [11]

Feature	Description	Abnormality Criteria
SBP	Systolic blood pressure	$SBP > 300mmHg$
DBP	Diastolic blood pressure	$DBP < 20mmHg$
PP	Pulse pressure	$PP < 20mmHg$
MAP	Mean arterial pressure	$MAP < 30mmHg$ or $MAP > 200mmHg$
T	Duration of each beat	
f	Heart rate (60/T)	$f < 20$ or $f > 200bpm$
ΔSBP	$SBP[k] - SBP[k-1]$	$\lvert\Delta SBP\rvert > 20mmHg$
ΔDBP	$DBP[k] - DBP[k-1]$	$\lvert\Delta DBP\rvert > 20mmHg$
ΔT	$T[k] - T[k-1]$	$\lvert\Delta T\rvert > 2/3sec$

PPG Signal Cleaning

The PPG signal quality is evaluated based on a Signal Quality Index proposed by Elgendi [48]. Elgendi compared eight different signal quality indices, and for lengths of PPG waveforms between 2 s and 30 s, the skewness Signal Quality Index (sSQI) method dementrated better performance than others. Skewness is a measure of the symmetry of a probability distribution and sSQI is is defined as:

$$S_{SQI} = 1/N \sum_{i=i}^{N} [x_i - \hat{\mu}_x/\sigma]^3 \tag{5.2}$$

where $\hat{\mu}_x/$ and σ are the empirical estimate of the mean and standard deviation of x_i, respectively, and N is the number of samples in the PPG signal [48] Using this method, the classifications of excellent waveforms versus acceptable or unfit were best when 5s was used as the window of the PPG waveform segment. Therefore, the sSQI is computed for each 5 second segment of the PPG signal. Segments with a value below zero are discarded. Flat segments where no signal is present are also removed.

5.1.4 Feature Extraction

The methodology followed to estimate blood pressure relies on the extraction of several features from the ECG and PPG signals, which have been used in previous studies with the same goal. All the features are described in tables 5.2, 5.3 and 5.4 and in figures 5.7, 5.8, 5.9 and 5.10. While many of these parameters are proposed in literature without explicit meaning, others have physiological meanings which have been described.

Pulse arrival time (PAT) corresponds to the time delay between the electrical activity of the heart and a peripheral pulse measured in a peripheral point in the arterial tree. [17]. This metric is defined in table 5.2 and figure 5.7.

Large artery stiffness index (LASI) is related to the transit time of pressure waves from the root of the subclavian artery to the apparent site of reflection and back to the subclavian artery [5]. This metric is computed as the time difference between systolic peak and inflection point, as defined in table 5.2 and figure 5.7.

The augmentation pressure (AG), measured by the augmentation index (AI), is the measure of the contribution that the wave reflection makes to the SBP, and it is obtained by measuring the reflected wave coming from the arterial tree periphery to the centre [5]. This metric is computed as the amplitude ratio of the inflection point to the systolic peak, as defined in table 5.2 and figure 5.7.

Table 5.2: Features computed from the PPG and ECG for each heart cycle

Feature	Description
PATf	time interval between the ECG R-peak and the PPG foot
PATd	time interval between the ECG R-peak and the PPG derivative maximum
PATp	time interval between the ECG R-peak and the PPG systolic peak
RR interval	Time interval between consecutive ECG R peaks
AI (Augmentation Index)	ratio of the height of the diastolic peak (x) to the systolic upeak (y) in the pulse $AI = \frac{x}{y}$
LASI (Large Artery Stiffness Index)	time delay between the systolic peak and the point of inflection
S1	Area under the curve (AUC) from start of cycle to max derivative point
S2	AUC from max derivative point to systolic peak
S3	AUC from systolic peak to diastolic rise
S4	AUC from diastolic rise to end of cycle

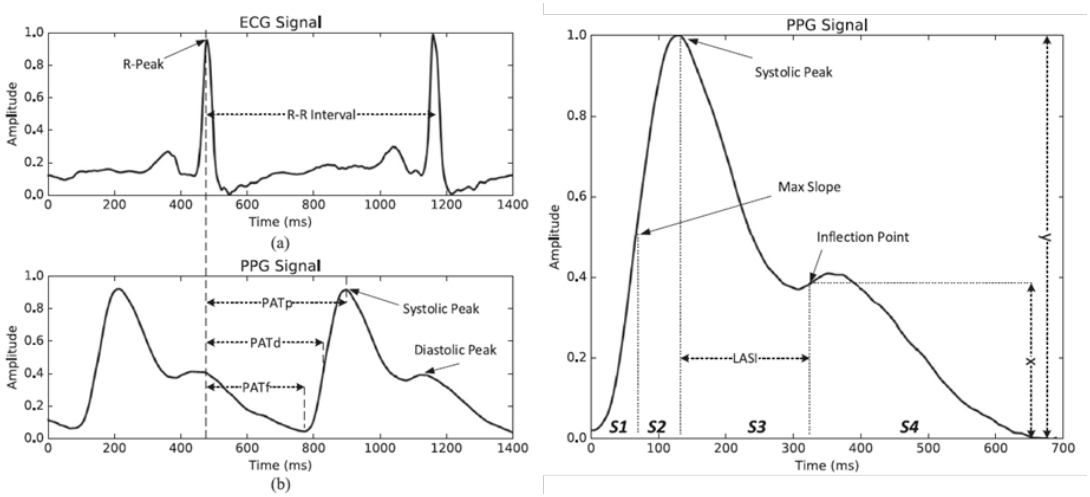

Figure 5.7: PPG and ECG features. The features are further described in table 5.2. Adapted from [7]

Systolic time, which is also known as crest time, has been proved useful for cardiovascular disease classification [5]. It is computed as the time difference between systolic peak and the PPG foot, as defined in table 5.3 and figure 5.8. The PPG characteristic value (PPGk) in table 5.3 is defined as

$$PPGk = \frac{p_m - p_f}{p_s - p_f} \tag{5.3}$$

where $p_m = \frac{1}{T}\int p_t dt$ and p_t gives the values of one cycle of the PPG signal as a function of time t, T is the duration of the cycle, p_s is the value at the systolic peak and p_f is the value at the foot of the waveform. PPGk was found to be a relevant feature for BP estimation by Miao et al. [8].

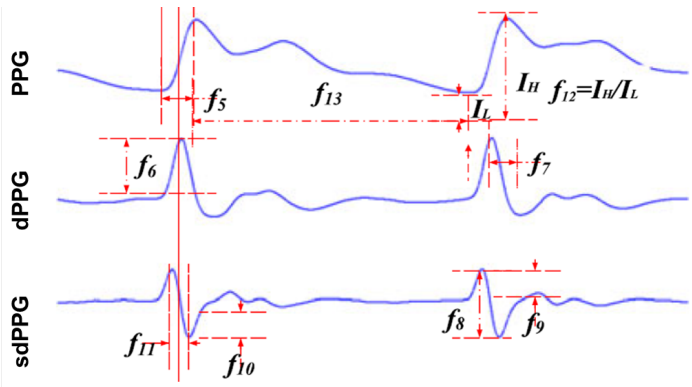

Figure 5.8: PPG signal (top), PPG signal derivative (middle) and PPG signal second derivative (bottom) with features identified: f5 – Systolic time; f6 – dPPGHeight; f7 – dPPGWidth; f8 – ppgSecondDeriHeight; f9 – sdPPGPeakHeight; f10 – sdPPGFootHeight; f11 – sdPPGWidth; f11 – sdPPGDeriWidth; f12 – PIR; f13 – Diastolic time, adapted from [8]

The second derivative of the PPG signal (sdPPG), an indicator of the acceleration of the blood in the finger, also contains commonly used features. The sdPPG signals is characterized by several peaks and

valleys respectively designated as a-wave (early systolic positive wave), b-wave (early systolic negative wave), c-wave (late systolic reincreasing wave), d-wave (late systolic redecreasing wave) and e-wave (early diastolic positive wave) [5]. The e-wave represents the dicrotic notch [5]. Analysis is usually performed in terms of the amplitudes of the b-, c-, d-, and e-waves with respect to the a-wave amplitude, illustrated in figure 5.9. The ratios computed are described in table 5.2.

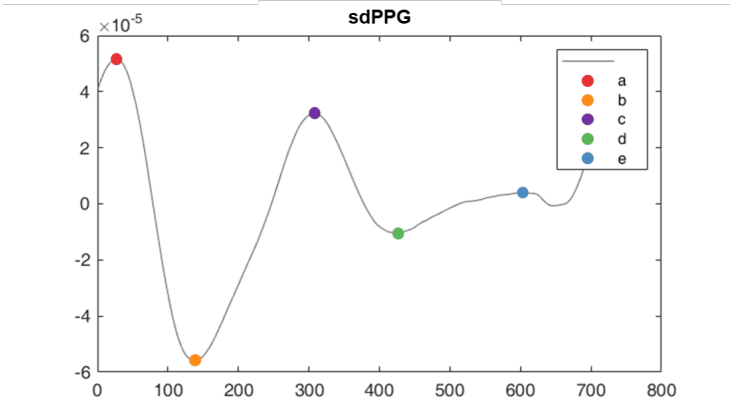

Figure 5.9: Waves in the PPG signal second derivative (sdPPG), namely a-wave (early systolic positive wave), b-wave (early systolic negative wave), c-wave (late systolic reincreasing wave), d-wave (late systolic redecreasing wave) and e-wave (early diastolic positive wave). The e-wave represents the dicrotic notch [5]

Table 5.3: Features computed from the PPG for each heart cycle

Feature	Description
Systolic time	Ascending time from PPG foot to PPG peak
dPPGHeight	Intensity of the first derivate of the PPG waveform
dPPGWidth	Time width of the first derivate of the PPG waveform
sdPPGHeight	Total intensity of the second derivate of the PPG waveform
sdPPGPeakHeight	Peak intensity of the second derivate of the PPG waveform
sdPPGFootHeight	Foot intensity of the second derivate PPG waveform
ppgSecondDeriWidth	Time width of the second derivate of the PPG waveform
PIR	Ratio of PPG peak intensity to PPG bottom intensity
Diastolic time	Descending time from PPG peak to PPG foot
PPGk	PPG characteristic value
b/a	ratio of the b-wave to the a-wave in the PPG second derivative (sdPPG)
c/a	ratio of the c-wave to the a-wave in the sdPPG signal
d/a	ratio of the d-wave to the a-wave in the sdPPG signal
e/a	ratio of the e-wave to the a-wave in the sdPPG signal

Finally, features that proved useful for risk stratification of hypertension on a study by Liang et al. [12] where also computed and are described in table 5.4 and figure 5.10, together with two extra area features.

Table 5.4: 11 features computed from the PPG, dPPG and sdPPG waveforms for each heart cycle. All the features except *area1* and *area2* are selected based on the study from Liang et al. [12]. The S, O, w, a, b, c and d variables with respective subscripts are illustrated in figure 5.10

Feature	Description
d	amplitude of the d wave in the sdPPG signal
powerAreaRatio1	ratio of the quadratic sum of the curve point from the S_{+1} point to c_{-1} point in the dPPG cycle to the quadratic sum of the dPPG cycle curve point $\left(\overbrace{S_{+1}c_{-1}} / \overbrace{O_{+1}O_{+1}}\right)$
powerAreaRatio2	ratio of the quadratic sum of the curve point from the S_{+1} point to d_{-1} point in the dPPG cycle to the quadratic sum of the dPPG cycle curve point $\left(\overbrace{S_{+1}d_{-1}} / \overbrace{O_{+1}O_{+1}}\right)$
amplitudeRatio1	ratio of the point in the PPG cycle corresponding to the c-wave peak to the systolic peak amplitude (S) (c_{-2}/S)
amplitudeRatio2	ratio of the point in the dPPG cycle corresponding to the c-wave peak to the max derivative point (w) (c_{-1}/w)
amplitudeRatio3	$((b-c-d)/a)$
timeSpan1	time span between the systolic peak (S) and the c_{-2} point in the PPG cycle $\left(\overline{Sc_{-2}}\right)$
slope1	slope from the b_{-2} point to the d_{-2} point $\left((b_{-2}-d_{-2})/\overline{b_{-2}d_{-2}}\right)$
slope2	slope from the systolic peak (S) to the d_{-2} point $\left((S-c_{-2})/\overline{Sc_{-2}}\right)$
area1	Area under the curve (AUC) from start of cycle to systolic peak (S1+S2)
area2	AUC from systolic peak to end of cycle (S3+S4)

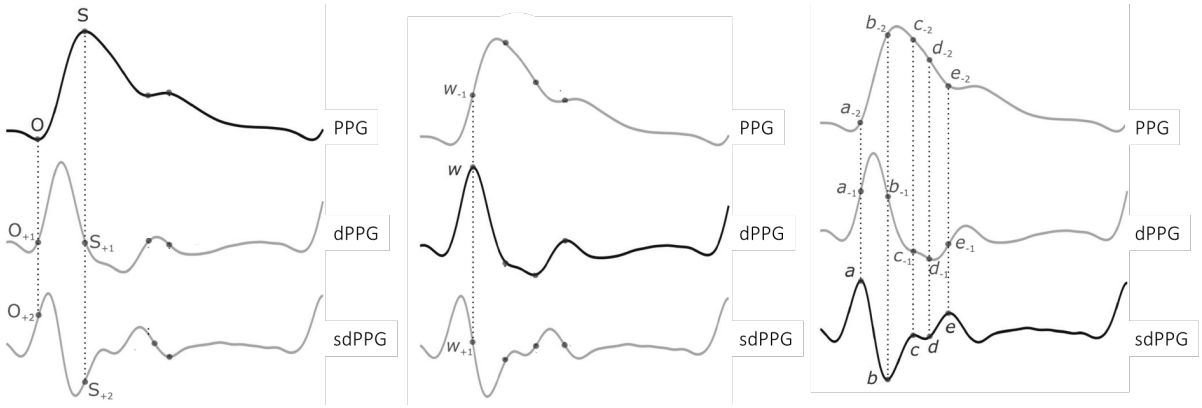

Figure 5.10: Definition of the fiductial points in PPG and its derivatives (dPPG and sdPPG) used to compute the features in table 5.4 and respective mapping to PPG, dPPG and sdPPG. S correspond to the systolic peak, O is PPG foot and w is the max derivative point ((adapted from [9]

The feature extraction process requires several substeps, as illustrated in figure 5.11, which will be described bellow.

Figure 5.11: Feature extraction process, corresponding to step (b) in the block diagram in figure 5.3

Beats Identification

Systolic peaks are first computed using an automatic multiscale-based peak detection (AMPD) algorithm [49]. The next step is to identify the points that mark the beginning of the PPG cycle (PPG foot), which are defined as the minimum value between two consecutive systolic peaks.

Beats Selection

Since some parts of the signal may contain low quality PPG cycles, a method to detect and remove them is necessary.

For this process, the signal is divided in 1 min segments, and the following steps are followed:

- Template creation: a template is computed as average of 30 seconds of beats (T1); The beats of that 30 seconds window that have a correlation coefficient lower than 0.85 with the template are excluded
  - If more than $\frac{1}{4}$ of the beats are excluded, the template is not used (If a previous template is available it is used instead; Else, a new one is computed from the next 30 seconds)
  - Otherwise, a new template is computed with the remaining beats (T2);
- Template comparison: All the beats in the 1 minute window are compared to the template and if the correlation coefficient is lower than 0.95 they are excluded An example of the result of this process is shown in figure 5.12.

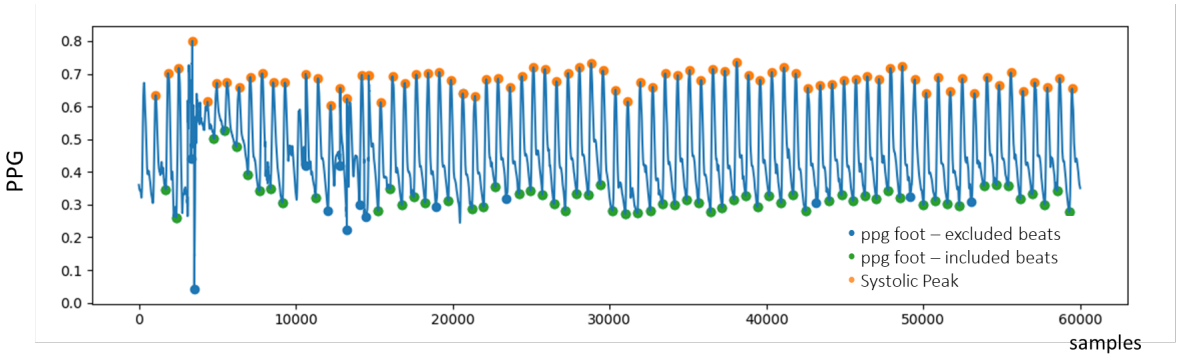

Figure 5.12: PPG segment with systolic peaks and the begging of each PPG cycle (PPG foot) identified. The cycles marked with a blue dot were excluded in the beat selection process, whereas the green marked cycles are considered to have good quality for feature extraction.

Computing features

To compute the features described above, several fiducial points need to be computed from the ECG, PPG, first derivative of the PPG (dPPG) and sdPPG signals. These include the R peaks in the ECG,

peaks in the ECG, which are detected using the Pan-Thompkins algorithm, the PPG foot, the systolic peaks, the max derivative points (dPPG maximum) and inflection points in the PPG signal.

The max derivative point is defined as the time value with greater gradient between the cycle start and the systolic peak.

The inflection point is defined as the largest peak in the PPG gradient between the systolic peak and the start of the next cycle. An example of the points computed is shown in figure 5.13.

Finally, to avoid the effects of noise, all features are averaged over 10 seconds segments, including blood pressure labels, so that only one value of each systolic blood pressure (SBP) and diastolic blood pressure (DBP) is estimated for each segment.

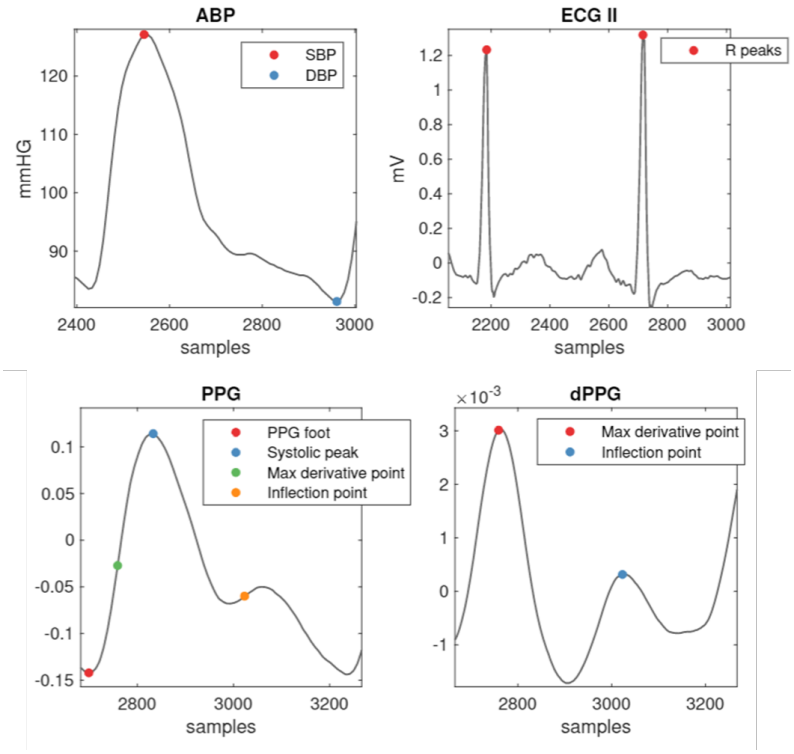

Figure 5.13: Example of PPG, ECG and ABP points identification. In ABP the systolic (SBP) and diastolic (DBP) BP values are identified. In the ECG signal, the R peaks are identified and in the PPG signal, the PPG foot, Systolic Peak, maximum of the first derivative (Max Derivative point) and Inflection point are identified. In the PPG first derivative signal, the points identified to detect the maximum of the first derivative (Max Derivative point) and Inflection point in the PPG signal are also shown.

5.2 WARD Data

In the WARD project, several physiological signals are acquired. ECG, PPG and blood pressure are the particular ones of interest to this project so the acquisition process and characteristics of these signals is described bellow.

ECG

The ECG signal acquisition is performed with Lifetouch Blue. The Lifetouch Blue is a continuous cardiac sensor that monitors the patient ECG with a sampling frequency of 1000 Hz and performs real time streaming of data via bluetooth. Before transmission, it performs signal processing consisting of QRS complexes detection and estimation of RRI, HR and respiration rate. QRS detection is based on a modified version of the open source ECG algorithm by EP limited. The raw ECG-signal is downsampled before streaming, resulting in a signal sampled at 100 Hz, and it is only transmitted for around 10 seconds each minute.

PPG

The PPG signal is acquired by Nonin WristOx2 pulse oximeter, which also provides oxygen saturation and pulse rate measurements. As with ECG, raw-PPG is not transmitted continuously, but only for about 10 seconds each minute, and its sampling frequency is 75 Hz. Part of the PPG data analysed, corresponding to 231 subjects, was acquired with 8-bit ADC, whereas data corresponding to other 108 was acquired with 12-bit ADC. By applying the BP estimation method to both data it will be possible to infer about the importance of data quality on the performance of the estimation method.

Blood Pressure

Since invasive ABP measurements are not recorded in the context of the WARD project, standard cuff-based blood pressure measurements are used instead as label for the blood pressure estimation algorithm. Blood pressure is recorded with TM2441 monitor.

TM2441 is an ambulatory blood pressure monitor also suitable for spot measurements in wards. It is a typical cuff based device, as it uses an oscillometric measurement method. It has been validated in accordance with ISO810601 protocol, and the pressure measurement accuracy is $\pm 3mmHg$. The range of measurement is 60 to 280 mmHg for systolic blood pressure and 30 to 160 mmHg for diastolic blood pressure.

In the WARD system, blood pressure is measured every 15, 30 or 60 minutes, and ECG and PPG signals are acquired continuously for 10 seconds each minute. Therefore, it was first necessary to select the ECG and PPG measurements from the same minute in which the blood pressure was measured. If any of the signals is missing, the measurement is rejected. The distribution of blood pressure values in the records selected from the WARD data

The steps implemented to estimate blood pressure from the WARD data are described in figure 5.14, and will be described in detail in the following sections.

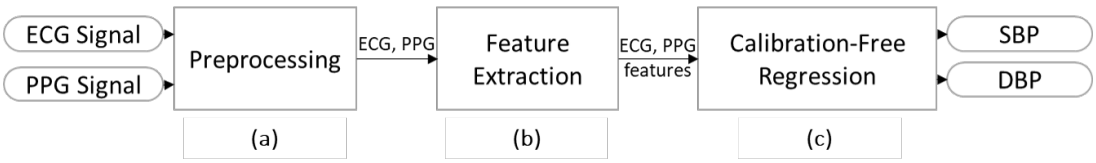

Figure 5.14: Block diagram of the proposed cuffless BP estimation method. Point measurements BP measurements obtained using a standard BP monitor to provide SBP and DBP values used as label. The steps in blocks (a), (b) and (c) are described in sections 5.2.1, 5.2.2 and 5.3, respectively.

5.2.1 Pre-processing

The PPG signal acquired by the Nonin WristOx2 pulse oximeter is often saturated at the maximum value so a cubic spline interpolation was performed on saturated signals, using a a window of 100 ms before and after the saturation zone. This process is illustrated in figure 5.15.

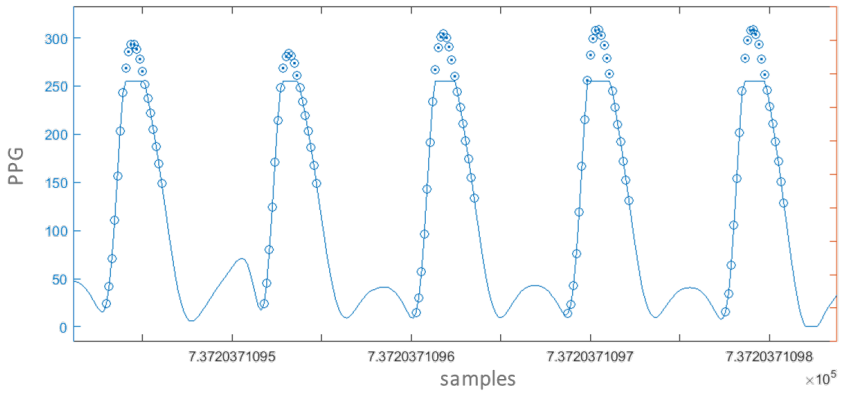

Figure 5.15: PPG signal reconstruction illustration. The blue circles (○) represent the samples 100ms sections before and after the saturation area and ⊙ the reconstructed peaks samples.

The PPG and ECG signals are then resampled from 75Hz and 100Hz, respectively, to 1000Hz using linear interpolation. The PPG and ECG signals are then filtered and denoised using discrete wavelet decomposition (DWT), following the method described is section 5.1.3. The PPG signal sections with low quality are also rejected according to the sSQI value, as described in section 5.1.3. Since the SBP and DBP values are obtained from a certified device, no pre-processing is necessary.

5.2.2 Feature Extraction

The features extracted are the same as those described in section 5.1.4, and a similar feature extraction process is followed, as explained in in the following subsections.

Beats Identification

Systolic peaks are computed using automatic multiscale-based peak detection (AMPD) algorithm [49] and the points that mark the beginning of the PPG cycle (PPG foot) are then defined as the minimum value between two consecutive systolic peaks.

Beats Selection

Since in the WARD data, the signals are not continuous, a modified approach is performed to identify noisy PPG cycles:

- Select last 30 seconds of measurements prior to BP measurement. An example is shown in figure 5.16.
- Template creation: a template is computed as average of the 30 seconds of beats (T1); The beats of that 30 seconds window that have a correlation coefficient lower than 0.85 with the template are excluded
  - If more than $\frac{1}{4}$ of the beats are excluded, the template is not used and a new one is computed from the previous 30 seconds of measurements
  - Otherwise, a new template is computed with the remaining beats (T2);
- Template comparison: All the beats in the 1 minute window are compared to the template and if the correlation coefficient is lower than 0.95 they are excluded

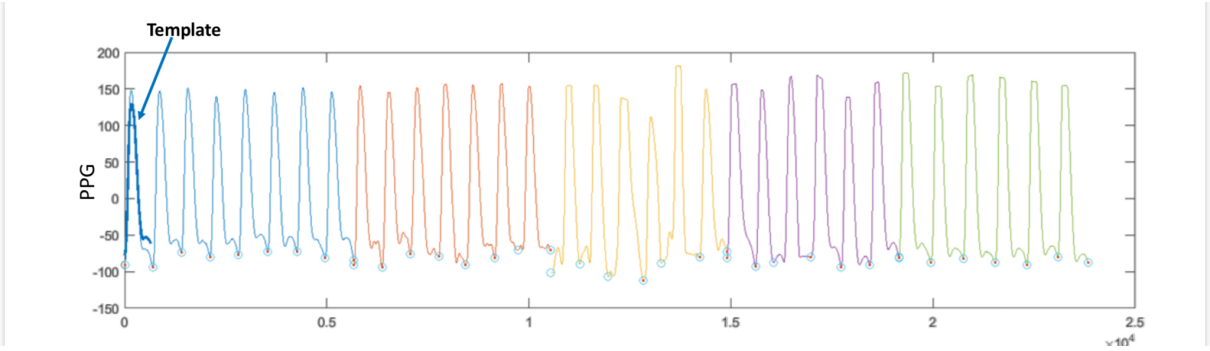

Figure 5.16: Template computed from WARD PPG measurements. Each color corresponds to a continuous measurement of the PPG signal (about 10 seconds) acquired in a distinct minute using the Nonin WristOx2 pulse oximeter.

Computing features

The ECG, PPG, dPPG and sdPPG signals fiductial points defined in section 5.1.4 are then computed. These list of points computed is as follows:

- R peaks in the ECG waveform
- PPG foot points in the PPG waveform
- Systolic peaks in the PPG waveform
- Max Derivative points in the PPG waveform
- Inflection points in the PPG waveform

Finally, to avoid the effects of noise, all features are averaged over the segments of around 10 seconds corresponding to the respective blood pressure label.

5.3 Regression algorithm

Random Forest

Random forests are an ensemble method which can be used for both classification and regression problems. The algorithm is based on a collection of decision trees.

Decision Trees are a supervised learning method used for classification and regression. The goal of the method is to split the training data into smaller subsets, in a way that the label variables in each subset are as homogeneous as possible. In each subset, the predictor is assumed to be constant and is defined as the most voted class [50].

In order to split the data, simple decision rules are learned from the data features. A tree is trained by choosing the best feature to split each node, starting from the root. The best feature to split node m is defined as the one that maximizes the impurity drop of the children nodes, with respect to node m. Several impurity measures are available, such as entropy and Gini index. The one used in this work is the Gini index, according to which the impurity of node m is defined as:

$$i(m) = -\sum_{k=1}^{K} P(k|m)(1 - P(k|m)) \tag{5.4}$$

where $P(k|m)$ is the proportion of class k observations in node m [50].

In random forests, each tree in the ensemble is built from a sample of the training set generated by bootstrap, that is, by sampling the training set with replacement. If k decision trees are generated, the random forest predictor is then formed by taking the average over k of the trees [51]. When splitting each node during the construction of a tree, the best split is found from a random subset of features. In this implementation, the number of features in the random subset is equal to one third of the total number of features. The purpose of these two sources of randomness is to decrease the variance of the forest estimator, since individual decision trees typically exhibit high variance and tend to overfit. The

randomness injected should create decision trees with prediction errors that can be cancelled out by taking an average of the respective predictions.

The Random Forest Regression algorithm was chosen for this implementation due to its robustness to noisy features and outliers. In addition, it has yield better results than other regression algorithms in studies which implemented several methods for comparison, such as those by Kachuee et al. [7] and Monte-Moreno [52]. Two estimation models were generated, by setting the training targets as SBP and DBP separately. A bagged regression tree algorithm was then used to generate a model, with the min leaf size set to 10 and the number of predictors to 100.

5.4 Model Evaluation

Since the amount of data used is limited, a 7-fold split was performed to evaluate the model. This is a trade-off between the typical test and train set split and a leave-one-subject-out (Leave One Subject Out (LOSO)) experiment. The latter consists of, in each of n iterations (n = the number of subjects), using the data of n-1 subjects for training, while the data of the left out subject is reserved for testing [53]. The advantages of this method is that the results should not depend on the split choice, which may lead to particularly optimistic or pessimistic results [53]. On the other hand, it highly increases computational complexity. Therefore, the data was instead separated in 7 groups, ensuring that data from each subject was only present in one of the groups. The model was then trained with 6 of the groups created and tested on the remaining group. This procedure is repeated 7 times, allowing all the data to be used for testing.

The agreement of estimated BP with the reference BP was evaluated using scatter plots, Bland–Altman plots, commonly used metrics such as the mean error, mean absolute error and root mean square error and blood pressure standards.

Bland-Altman plots

The Bland-Altman plot describes the agreement between two quantitative measurements, which in this case correspond to the true and estimated blood pressure measurements. It consists of a scatter plot where the difference of the two measurements is plotted against their mean value. Its analysis allows the quantification of the agreement between two measurements by studying the mean difference and constructing an agreement interval, within which 95% of the differences between the estimated and true blood pressure measurements fall.

Metrics

The mean error (ME), mean absolute error (Mean Absolute Error (MAE)) and root mean square error (Root Mean Square Error (RMSE)) are respectively defined as:

$$ME = \frac{1}{n}\sum_{i=1}^{n} y - y^* \tag{5.5}$$

$$MAE = \frac{1}{n}\sum_{i=1}^{n} |y - y^*| \tag{5.6}$$

$$RMSE = \sqrt{\frac{1}{n}\sum_{i=1}^{n} (y - y^*)^2} \tag{5.7}$$

where n is the number of instances, y the true BP value and y^* is the estimated value.

Blood pressure measurement standards

Performance was also evaluated based on the Advancement of Medical Instrumentation (AAMI) standard defined in section 4.4.2. To evaluate the model according to the standard, shown in table 4.1, it was also necessary to compute the standard deviation (STD) of the ME.

6

Blood Pressure Estimation Results

6.1 State of the art method implementation

The method implemented for comparison was trained on the 146 subjects from the MIMIC-II database. As observed in table 6.1, the results obtained were not as good as those implemented by Kachuee et. al [7]. The main reason behind this is that the parameter-based method, which has been implemented, is not suitable for signals with abnormal morphologies, making the extraction of physiological parameters unreliable in these cases. However, this study does not disclaim how the unsuitable signals are removed, so in the present implementation all the data described in section 5.1.1 were used. It also does not describe any method to reject noisy parts of the signals, for which attempting to extract features will lead to abnormal values.

Table 6.1: Results of implementing the state of the art method for cufless BP estimation by Kachuee et al. [7]

		ME (mmHg)	STD (mmHg)	Subjects
Kachuee [7]	DBP	0.36	5.70	942
	SBP	-0.06	9.88	942
Implemented Version	DBP	-1.3519	10.7213	98
	SBP	2.8224	21.9617	98

6.2 MIMIC II database

6.2.1 Total dataset

On a first step, the model was trained and tested on the total data extracted from 146 subjects from the MIMIC database using the 7-fold cross validation process described in the previous chapter. The data was first trained using only the 10 features described in [7] and in table 5.2 and figure 5.7. On a second stage including additional features inspired by other literature studies and physiological parameters that can be extracted from the PPG signal, namely those described in table 5.3. All the results are presented in table 6.2. All the performance metrics except the RMSE slighly decreased (ME, STD and MAE), pointing that including these extra features improves the algorithm performance. In addition, an example of feature importance for the 24-features model is also presented in figure 6.2.

When comparing the STD value for DBP in table 6.2 (13.35 mmHg) to that in the implemented version of the algorithm by Kachuee et al., in table 6.1 (10.72 mmHg), an increase deviation is observed, which is due to the fact that in the original algorithm, only DBP values in the range $60mmHg \geq DBP \geq 130mmHg$ are considered, which is a limitation.

Table 6.2: Results of implementing the blood pressure estimation method developed, described in chapter 5, using the data obtained from the MIMIC II database

		ME (mmHg)	STD (mmHg)	MAE (mmHg)	RMSE (mmHg)
10 features (table 5.2)	DBP	0.76	13.35	10.92	13.52
	SBP	1.22	19.92	16.52	20.30
24 features (tables 5.2 and 5.3)	DBP	0.48	12.76	10.81	13.55
	SBP	1.13	19.53	16.63	20.32

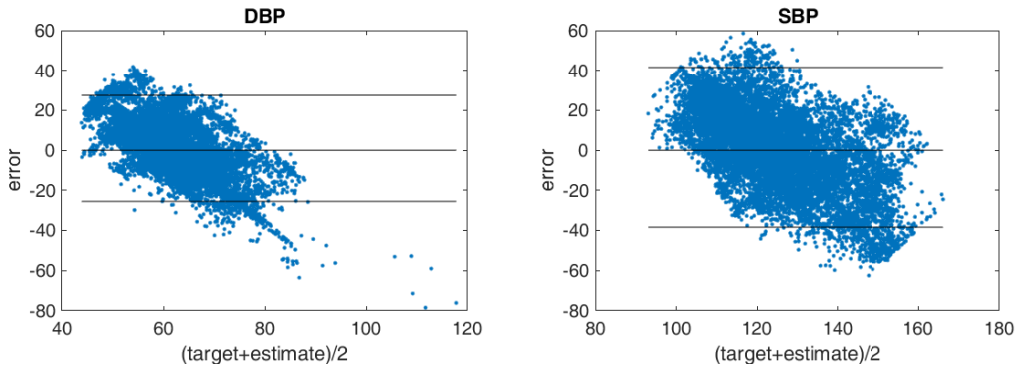

Figure 6.1: Bland-Altman plot for SBP and DBP estimation using the 24-features model on 146 subjects data from the MIMIC II database

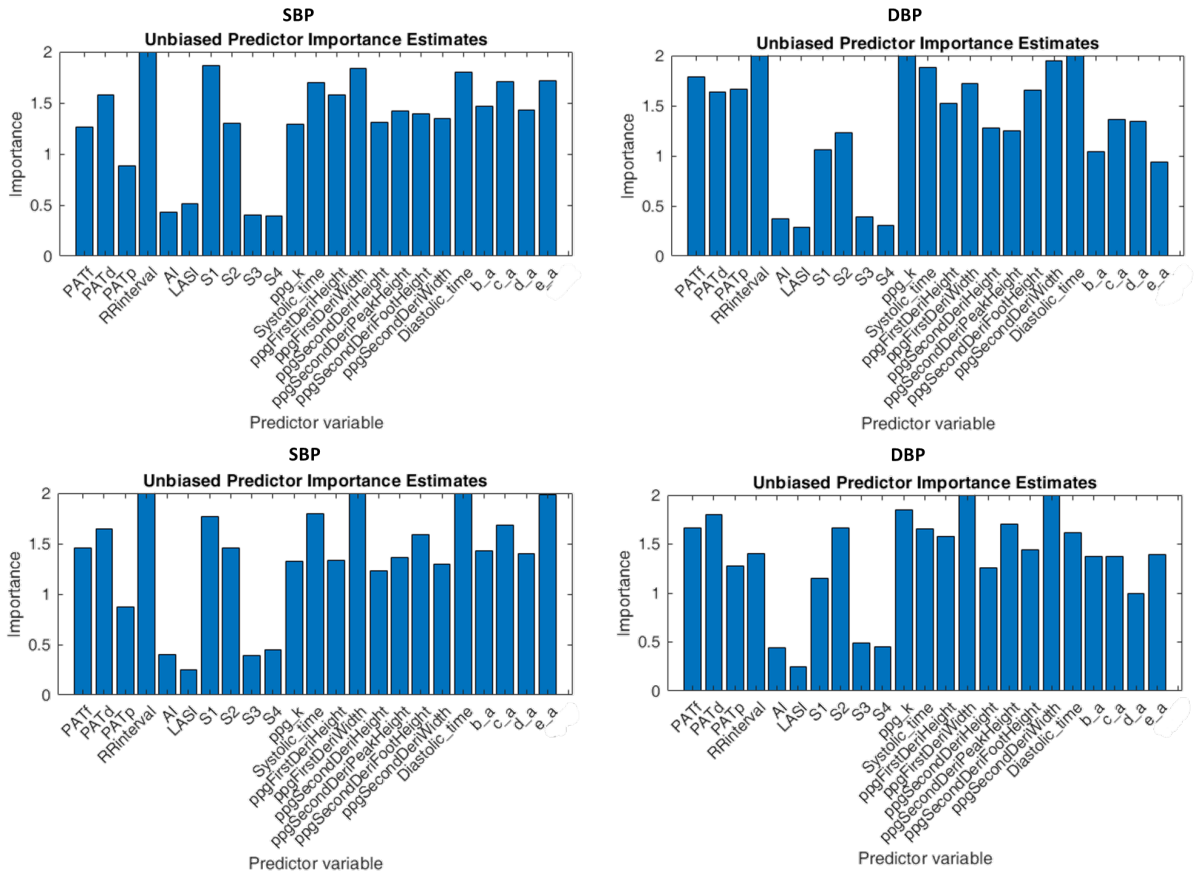

Figure 6.2: Feature importance for two of the SBP and DBP estimation models in the 7-fold training and testing procedure for using the 24-features model on 146 subjects data from the MIMIC II database. The features correspond to those described in tables 5.2 and 5.4

6.2.2 Good Quality Subset

Although the method developed is able to identify noisy sections of signals, it does not identify the PPG signal portions which do not have the typical shape, and the second wave and dichrotic notch are not detectable. This typically occurs in older patients, due to the increased artery stiffness, which are commonly monitored in the general ward. An example of this type of PPG signal is shown if figure 6.5b. It can be observed that there is no prominent maximum between two consecutive *Max derivative* points is the dPPG signal in figure 6.5b. Therefore, a substudy was conducted by training and testing the model on a small subset of data from 21 subjects that were visually considered to have good quality for feature extraction, as the one shown in figure 6.5a. The distribution of parameters in this subset is shown in figure 6.3. The model was trained using the LOSO approach described in the previous chapter, due to the reduced number of subjects present in the subset.

The model was trained with the initial 10 features in table 5.2, with both those features added to the ones in table 5.3 (the 24 feature model used for the total dataset) and with the total 35 features from

tables 5.2, 5.3 and 5.4. The results obtained are shown in table 6.3 and the Bland-Altman plots in figure 6.4 for the best performing method, with 24 features. It was observed that the 36 features did not result in a significant improvement compared to the 24 features model, so it was not applied to the total dataset.

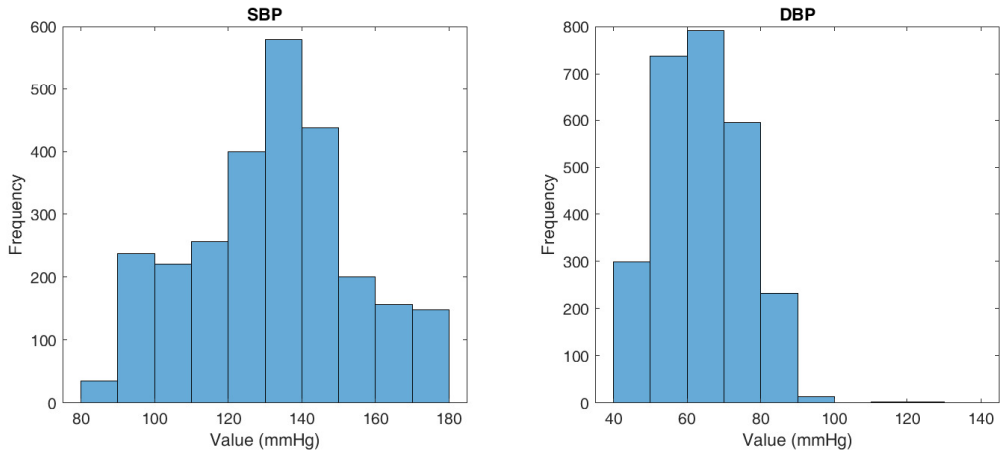

Figure 6.3: Distribution of parameters for 21 subjects: systolic blood pressure (SBP) and diastolic blood pressure (DBP)

Table 6.3: Results of implementing the blood pressure estimation method developed, described in chapter 5, using a good quality subset of data obtained from the MIMIC II database

		ME (mmHg)	STD (mmHg)	MAE (mmHg)	RMSE (mmHg)
10 features (table 5.2)	DBP	11.55	6.34	15.03	16.18
	SBP	0.51	9.27	20.58	22.44
24 features (tables 5.2 and 5.3)	DBP	5.20	5.13	10.61	11.82
	SBP	1.70	7.98	17.38	19.18
35 features (tables 5.2, 5.3 and 5.2)	DBP	6.25	5.63	11.08	12.40
	SBP	0.27	7.92	17.72	19.46

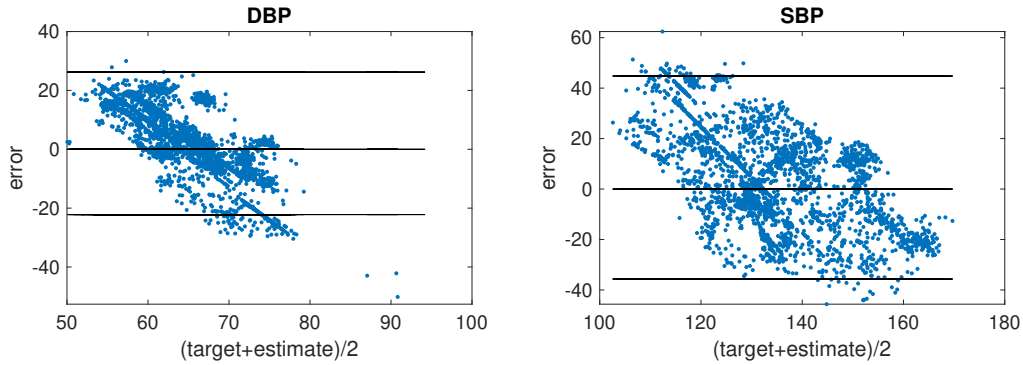

Figure 6.4: Bland-Altman plot for SBP and DBP estimation using the 24-features model on 21 subjects data from the MIMIC II database

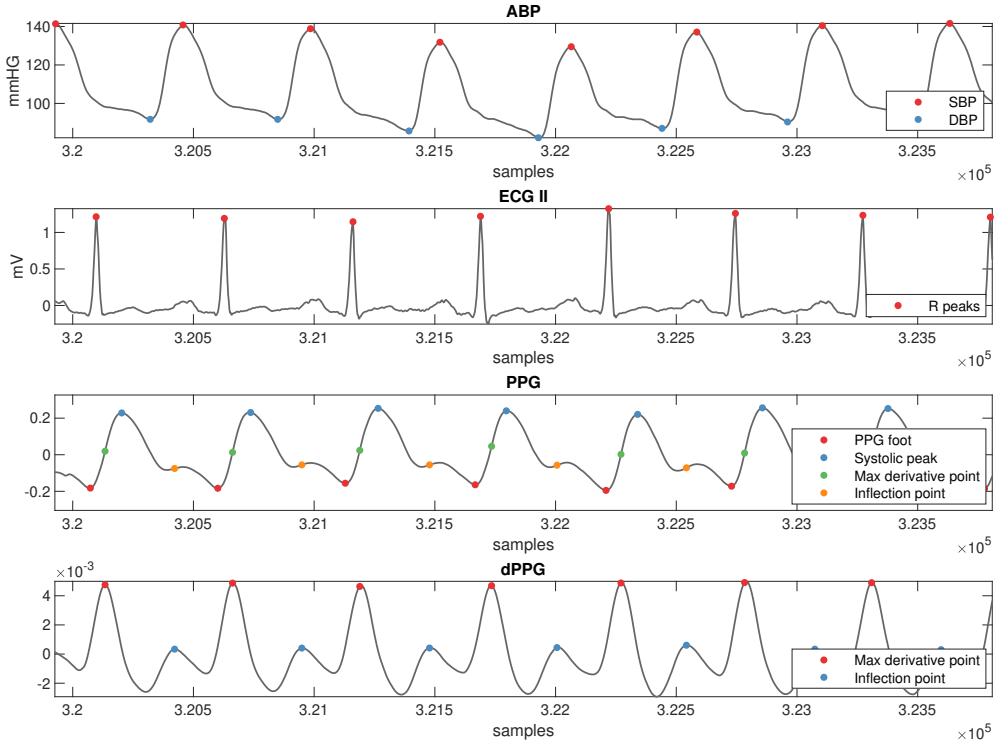

(a)

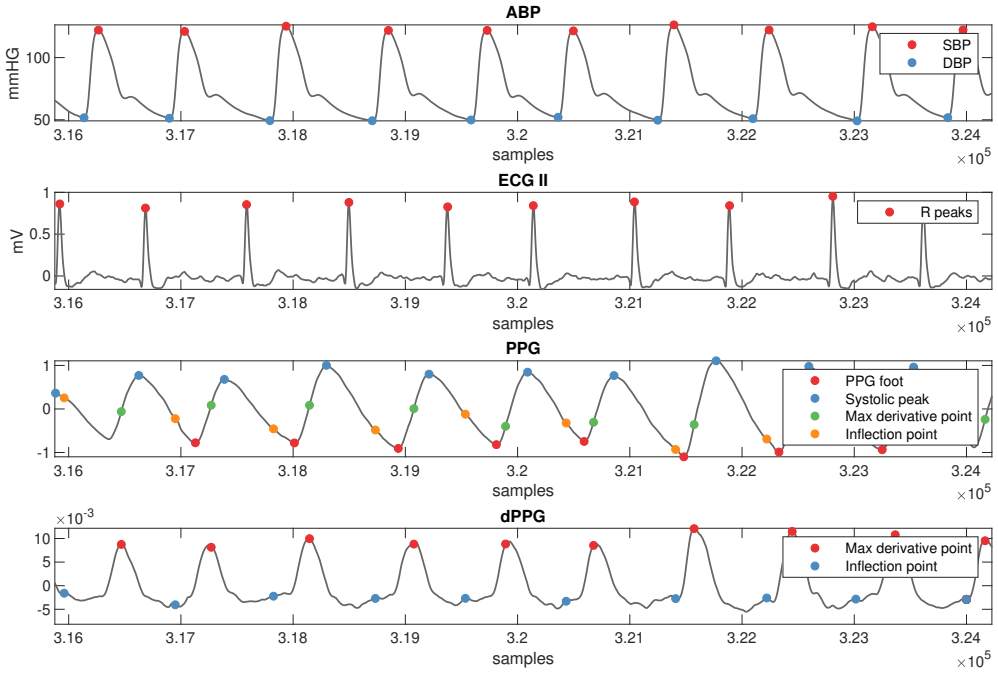

(b)

Figure 6.5: Patient records segment containing ABP, ECG and PPG. The first derivative of the PPG signal is also displayed, showing the peaks corresponding to the *Inflection point* and *Max derivative point*, the maximum of the first derivative in each PPG cycle; (a) good quality segment, in which the dichrotic notch in the PPG signal is easily detected. (b) abnormal record, in which the dichrotic notch in the PPG signal is not easily distinguished.

6.3 WARD data

The outcomes of applying the model to the data collected by the WARD monitoring system can only be qualitatively described, as unpublished data from the WARD patient cohorts has been used. The same performance metrics used in the MIMIC II results evaluation were also computed (namely, ME, STD, MAE and RMSE) and the values were comparable to those obtained in the total dataset from the MIMIC II database. As in the total MIMIC II dataset, the STDs of the estimation errors do not comply with the AAMI sandard for SBP and DBP estimation. However, the PPG data with higher resolution (12 bit ADC) allowed improved results compared to the PPG data with lower resolution (8 bit ADC), as expected. In both data sets the estimation results are poorer for the extreme values (low and high blood pressure).

The application to the WARD data of the data selection and cleaning procedures, described in the previous chapter, resulted in a large decrease in the number of measurements available for training and testing the BP estimation algorithm. In particular, the available measurements from the lower resolution subset decreased to about 12 % of the initial number of measurements. For the higher resolution subset, the available measurements decreased to about 20 %. This means that in the best case, it would be possible to estimate blood pressure about 12 times per hour (20 % of the minute-based signal acquisitions).

7

Discussion

In this chapter, the results obtained are discussed and compared with state of the art studies. Possible sources of error are also presented and their implications are discussed.

7.1 Available data

One of the main factors influencing the results of the study conducted is the quality of the available data. Therefore, the characteristics of the data available and their implications are discussed in this section.

7.1.1 MIMIC database

Data from the MIMIC database has the advantage of having invasive ABP waveforms available, from which SBP and DBP values can be extracted with high precision given that it is the standard for validation of new BP measurement technologies. However, this data is mainly obtained from critically ill patients, having possible medical conditions that alter the PPG waveform, making the extraction process of a number of features less accurate. In particular, for people with arterial stiffness or stage III hypertension,

as may occur in the older population, the PPG waveform may lose some important features such as its dicrotic notches, making the estimation less precise [4].

On the other hand, there are few measurements with low or high blood pressure values, as observed in the histogram in figure 5.2, making it difficult to obtain accurate measurements in the limits of the physiological range. In particular, the ABP data do not provide values above 180 mmHg. Another problem that affects the performance of the BP estimation model is that, as mentioned in the previous chapter, the ECG and PPG signals are often not synchronized, making the PAT features inaccurate. For this reason, it was also not possible to implement any literature method based solely on the PAT or PTT features, although this methods have shown promising performance in estimating blood pressure, as shown in chapter 4.

7.1.2 WARD project

About 700 patients have been monitored with the WARD system, and it was possible to obtain thousands of blood pressure measurements with simultaneous PPG and ECG signals, thus showing great potential for the training and testing of a blood pressure estimation model.

However, on a first approach, several problems were detected, namely the lack of synchronicity between the ECG and PPG signals. Since these are acquired for only 10 seconds each minute, if the PPG and ECG segments are not simultaneous it is not possible to extract information for BP estimation. In addition, the PPG signals with 8 bit resolution often lack sufficient quality to extract any reliable features, particularly when the amplitude is low. These problems appear to be less severe on the second set of data, in which the PPG waveform has a 12 bit resolution. However, only for 108 of the subjects monitored the signals have such characteristics. It should be noted that even in this second set of data, there are synchronicity problems, introducing errors in the PAT features extracted. Therefore future improvements of the acquisition system to provide synchronous ECG and PPG signals would benefit the accuracy of the estimation system.

7.2 Data pre-processing and shut down algorithm

The use of a clinical database implies some difficulties such as a high presence of noise and motion artifacts, and the possibility that not all of the signals are available for the whole duration of the records. This created the need for several data pre-processing steps. Namely, the PPG signal was processed using wavelet denoising, the low quality segments were removed based on the sSQI value and the low quality cycles from PPG were removed by comparing each cycle with a template, calculated using all cycles in a windows of time. The aim was to maintain only the cycles that are not influenced by motion artifacts and other conditions that change the typical shape of the cycles. The resulting signal segments

were then used to compute a set of features. It was observed that when features are computed after sSQI selection and template cleaning, less outliers are obtained.

7.3 Comparison with State of the Art Studies

The results of implementing the state of the art method by [7] showed a performance inferior to the one obtained in such study. For DBP the mean error obtained was $-1.35 \pm 10.72 mmHg$ compared to $0.36 \pm 5.70 mmHg$ and for SBP it was $2.82 \pm 21.96 mmHg$ compared to $-0.06 \pm 9.88 mmHg$ in the original paper. The main reason behind this is the lack of reliability in the feature extraction process for signals with abnormal morphologies. This study does not disclaim how the unsuitable signals are removed, so in the version implemented, all the data described obtained from the MIMIC database were used. It also does not describe any method to reject noisy parts of the signals in which attempting to extract features will lead to abnormal values.

In table 7.1, a comparison between this work and the state of the art methods discussed in chapter 4 is shown. It is generally difficult to compare results from the various state of the art studies, due to different evaluation metrics and varied datasets whose characteristics are often not specified. In addition, it should be taken into account that the methods requiring calibration generally have lower errors. Particularly, the Ding method shows a error of only $-0.40 \pm 7.11 mmHg$ for DBP and $1.17 \pm 5.72 mmHg$, being the only method of those stated that complies with the AAMI standard regarding STD. However, one of the problems of calibration is that its accuracy may deteriorate over time, and the intervals at which a new calibration is necessary are not studied.

Lower errors are also observed in small selected subsets of data while work including large scale data has larger errors, which was also observed in this project. This highlights the difficulty of creating a robust general model on a large dataset, possibly containing subjects with varied characteristics. Another reason for this problem, pointed by Slapnicar et al. [53], is that the large MIMIC III dataset may as well contain data from different PPG and ABP measurement devices.

All the results obtained in this project meet the AAMI standard regarding mean error (ME) except DBP for the good quality subset in the MIMIC II database. In this particular case ME was $5.20 mmH$ which is only slightly above the limit of the standard ($5 mmHg$). This could be due to the distribution of DBP measurement values, observed in figure 6.3. As for standard deviation (STD), only in the small subset the values are inferior to the AAMI standard of $8 mmHg$.

Table 7.1: Comparison with state of the art methods.

	DBP			SBP			Number of test subjects
	ME $\pm$ STD (mmHg)	MAE (mmHg)	RMSE (mmHg)	ME $\pm$ STD (mmHg)	MAE (mmHg)	RMSE (mmHg)	
Salpnicar et al. [53]	-	13.62	-	-	18.34	-	510
Xing et al. [4]	2.6 ± 9.3	-	-	5.5 ± 15.5	-	-	1532
Ding et al. [22]	0.40 ± 7.11	-	-	1.17 ± 5.72	-	-	33
Kachuee et al. [7]	0.36 ± 5.70	-	-	-0.06 ± 9.88	-	-	942
Kachuee et al. implemented version	-1.35 ± 10.72	5.83	-	2.82 ± 21.96	11.80	-	942
MIMIC II data	5.20 $\pm$ 5.13	10,61	11.82	1.70 $\pm$ 7.98	17.38	19.18	21
MIMIC II data	0.48 $\pm$ 12,76	10,81	13,55	1.13 $\pm$ 19,53	16,63	20,32	146
AAMI standard	$\leq 5 \pm 8$	-	-	$\leq 5 \pm 8$	-	-	85

7.4 Potential of cuffless continuous SBP and DBP estimation

The research conducted shows potential for estimation of BP without a cuff based device. However, before this algorithm is to be applied to the WARD system it is necessary to improve its accuracy in the lower and higher values of the blood pressure range. The event classes requiring BP measurements, namely hypotension, circulatory failure and hypertension are defined based on SBP in the limits of the physiological ranges (SBP > 180 mmHg and SBP < 91 mmHg), where the estimation algorithm shows decreased performance.

Since for the blood pressure limit values a very precise value is not absolutely necessary, as it would only be necessary to know whether the values are in the abnormal ranges or not, a possible upgrade of the developed algorithm could be to perform classification instead of regression. However, this could give rise to problems in the case of values close to the classification, whereas a regression algorithm with good performance would be more precise. Redefining the limit values to compensate this issue could also present problems. Defining a lower limit for DBP and higher for SBP could lead to potentially missing risk situations, whereas a higher limit for DBP and lower limit for SBP could lead to false alarms.

Another issue referred in the previous chapter is the influence of the accuracy in detecting the dicrotic notch. As observed in figure 6.2, the features based on the time position or amplitude of the dicrotich notch revealed to be less important. This was particularly relevant because in both datasets, elderly and diseased patients are common. Therefore, this features show little potential for continuous SBP and DBP estimation in the scope of the WARD project, unless an alternative way to estimate the dicrotic notch is developed.

Although the PPG and ECG signals are currently acquired each minute by the WARD system de-

vices, blood pressure estimation cannot be obtained with the same frequency, since these signals often contain noise. However, it is still possible to increase the rate of measurements when compared to the cuff based device currently in use, with the advantage of decreasing the apparatus required to monitor the patients, and also making it more comfortable. As referred in the previous chapter, with the current data pre-processing pipeline, it would be possible to obtain about 12 measurements per hour, which is a good improvement comparing to the current system (measurements performed every 15 or 30 minutes during the day)

Lastly, the use of signals from two different devices in the method developed, namely the PPG and the ECG signals, is often seen in literature as a disadvantage, since it is less convenient for the patient when compared to having only a single device. However, for the current system, ECG and PPG are already monitored for other purposes, and do not represent an increase in the apparatus required to monitor blood pressure. Also PAT and PTT are well studied and have been proven to be correlated with systolic and diastolic BP. Therefore, these features are useful to improve the performance of the BP estimation model.

8

Conclusions

The main aim of this project was to develop a blood pressure estimation method that could be applied to the data acquired by the WARD system to monitor patients admitted to general WARD.

The first goal was to conduct a state of the art research regarding existing cuffless blood pressure estimation methods. It was found that there many recent developments in this field although the ones validated in a sufficiently large number of subjects do not yet meet the standards for clinical application. In addition, the methods achieving better performances often include a calibration procedure requiring a variation in the subject's blood pressure. This is not feasible in cases such as the one studied in this project, in which the subjects are hospitalized. The most relevant studies were therefore selected based on performance results, number of subjects in which they were evaluated and the absence of calibration.

The second goal was to implement different state of the art approaches to cuffless blood pressure estimation. Although the methods based on physiological models relating PAT or PTT features to BP have shown promising performance,the implementation of any of these was not feasible due to lack of synchronization between ECG and PPG signals. Taking into account the characteristics of the literature studies, the data-driven method by Kachuee et al. [7] was chosen to be implemented.

The third goal was to propose and test improvements to the current methods. The main improve-

ments implemented and tested were the extra features extracted from the PPG morphology and the steps of data preprocessing allowing to obtain only clean sections of the PPG signal, which lead to an improvement in the estimation performance. Although even with the additional steps developed it was not possible to achieve results comparable to the best performances in the literature, it was possible to improve the performance compared to the initial state of the art method implemented. Additionally, satisfactory results were obtained in a small subset of patients.

The fourth goal was to apply the methods implemented to the patient dataset acquired in the WARD project, providing a more reliable validation compared to the state of the art methods. This was also possible, although large errors pointing at issues related to signal quality, commonly encountered in the elderly patients, who make most of the population in the WARD project.

The fifth goal was to discuss the value of the development of a cuffless blood pressure measuring device. Having a method that allows blood pressure estimation would extremely be valuable, particularly in the setting of the WARD project, in which patients need to have blood pressure evaluated often. However, it is important to ensure the accuracy of the method, particularly in the extreme values of blood pressure.

8.1 Future Work

One of the crucial points in the development of an accurate algorithm for the estimation of blood pressure, is to have an effective shut down algorithm. Artifacts are one of the weaknesses in using the PPG for diagnosis, since the noise can limit the reliability and practical implementation of real-time monitoring applications [48]. Artifacts can result in loss of data, inaccurate readings, and false alarms, affecting the accuracy of pulse oximetry.

In the context of blood pressure estimation, it is important to identify and reject noisy and low quality PPG segments to prevent inaccurate BP estimation. Although random forest regression is robust to noisy features, it is important to decrease their occurrence since it affects the performance of the trained model. Other metrics such as kurtosis and perfusion have been proposed for the estimation of signal quality is the PPG signal [48]. Therefore, a combination of these metrics could be a way to improve the detection of low quality segments. It is also important to tune the thresholds of the metrics used to separate good quality and low quality PPG, for which a dataset of PPG segments labeled by experts would be necessary.

Another point to be improved is the automatic detection of PPG fiductial points. In the developed system, the systolic peaks are detected with the AMPD algorithm, which is robust to artifacts is most cases. However, the other fiductial points are detected using simple methods based on detecting maximum and minimum points in the PPG first and second derivative. This works well for waveforms with well defined

dicrotic notches and in the absence of noise. However, in the remaining cases, more robust methods would allow a more accurate determination of these points. In particular, Elgendi et al. [54] have proposed a method to improve the detection of the a-waves in the sdPPG waveform. The integration of such improvements in the current system should result in a better performance.

Bibliography

[1] S. M. Rasmussen, "Automatic Detection of Arrhythmias for Real Time Monitoring of Inpatients," Ph.D. dissertation, Technical University of Denmark, 2019.

[2] L. L. &. OpenStax, "Anatomy and physiology ii." [Online]. Available: https://courses.lumenlearning.com/suny-ap2/chapter/blood-flow-blood-pressure-and-resistance-no-content/

[3] G. Ogedegbe and T. Pickering, "Principles and Techniques of Blood Pressure Measurement," *Cardiology Clinics*, vol. 28, no. 4, pp. 571–586, 2010.

[4] X. Xing, Z. Ma, M. Zhang, Y. Zhou, W. Dong, and M. Song, "An Unobtrusive and Calibration-free Blood Pressure Estimation Method using Photoplethysmography and Biometrics," *Scientific Reports*, vol. 9, no. 1, pp. 1–8, 2019.

[5] M. Elgendi, "On the Analysis of Fingertip Photoplethysmogram Signals," *Current Cardiology Reviews*, vol. 8, no. 1, pp. 14–25, 2012.

[6] Y. Liang, D. Abbott, N. Howard, K. Lim, R. Ward, and M. Elgendi, "How Effective Is Pulse Arrival Time for Evaluating Blood Pressure? Challenges and Recommendations from a Study Using the MIMIC Database," *Journal of Clinical Medicine*, vol. 8, no. 3, p. 337, 2019.

[7] M. Kachuee, M. M. Kiani, H. Mohammadzade, and M. Shabany, "Cuffless Blood Pressure Estimation Algorithms for Continuous Health-Care Monitoring," *IEEE Transactions on Biomedical Engineering*, vol. 64, no. 4, pp. 859–869, 2017.

[8] F. Miao, N. Fu, Y. T. Zhang, X. R. Ding, X. Hong, Q. He, and Y. Li, "A novel continuous blood pressure estimation approach based on data mining techniques," *IEEE Journal of Biomedical and Health Informatics*, vol. 21, no. 6, pp. 1730–1740, 2017.

[9] M. Elgendi, Y. Liang, and R. Ward, "Toward Generating More Diagnostic Features from Photoplethysmogram Waveforms," *Diseases*, vol. 6, no. 1, p. 20, 2018.

[10] P. K. Whelton, R. M. Carey, W. S. Aronow, D. E. Casey, K. J. Collins, C. D. Himmelfarb, S. M. DePalma, S. Gidding, K. A. Jamerson, D. W. Jones, E. J. MacLaughlin, P. Muntner, B. Ovbiagele,

S. C. Smith, C. C. Spencer, R. S. Stafford, S. J. Taler, R. J. Thomas, K. A. Williams, J. D. Williamson, J. T. Wright, G. N. Levine, P. T. O'Gara, J. L. Halperin, I. Past, S. M. Al, J. A. Beckman, K. K. Birtcher, B. Bozkurt, R. G. Brindis, J. E. Cigarroa, L. H. Curtis, A. Deswal, L. A. Fleisher, F. Gentile, Z. D. Goldberger, M. A. Hlatky, J. Ikonomidis, J. A. Joglar, L. Mauri, S. J. Pressler, B. Riegel, D. N. Wijeysundera, M. N. Walsh, S. Jacobovitz, W. J. Oetgen, M. A. Elma, A. Scholtz, K. A. Sheehan, A. R. Abdullah, N. Tahir, J. J. Warner, N. Brown, R. M. Robertson, G. R. Whitman, and J. Hundley, "2017 ACC/AHA/AAPA/ABC/ACPM/AGS/APhA/ ASH/ASPC/NMA/PCNA guideline for the prevention, detection, evaluation, and management of high blood pressure in adults a report of the American College of Cardiology/American Heart Association Task Force on Clinical practice guidelines," *Journal of the American College of Cardiology*, vol. 71, no. 6, pp. E13–E115, 2018.

[11] J. X. Sun, A. T. Reisner, and R. G. Mark, "A signal abnormality index for arterial blood pressure waveforms," *Computers in Cardiology*, vol. 33, pp. 13–16, 2006.

[12] Y. Liang, Z. Chen, R. Ward, and M. Elgendi, "Hypertension Assessment Using Photoplethysmography: A Risk Stratification Approach," *Journal of Clinical Medicine*, vol. 8, no. 1, p. 12, 2018.

[13] A. K. Khanna, P. Hoppe, and B. Saugel, "Automated continuous noninvasive ward monitoring: Future directions and challenges," *Critical Care*, vol. 23, no. 1, pp. 1–5, 2019.

[14] F. Michard, D. I. Sessler, and B. Saugel, "Non-invasive arterial pressure monitoring revisited," *Intensive Care Medicine*, vol. 44, no. 12, pp. 2213–2215, 2018.

[15] R. Mukkamala, J. O. Hahn, O. T. Inan, L. K. Mestha, C. S. Kim, H. Toreyin, and S. Kyal, "Toward Ubiquitous Blood Pressure Monitoring via Pulse Transit Time: Theory and Practice," *IEEE Transactions on Biomedical Engineering*, vol. 62, no. 8, pp. 1879–1901, 2015.

[16] M. Elgendi, R. Fletcher, Y. Liang, N. Howard, N. H. Lovell, D. Abbott, K. Lim, and R. Ward, "The use of photoplethysmography for assessing hypertension," *npj Digital Medicine*, vol. 2, no. 1, pp. 1–11, 2019.

[17] J. Solà and R. Delgado-Gonzalo, *The Handbook of Cuffless Blood Pressure Monitoring, A Practical Guide for Clinicians, Researchers, and Engineers*. Springer Nature Switzerland AG, 2019.

[18] C. L. Duus, E. K. Aasvang, R. M. Olsen, H. B. Sørensen, L. N. Jørgensen, M. P. Achiam, and C. S. Meyhoff, "Continuous vital sign monitoring after major abdominal surgery—Quantification of micro events," *Acta Anaesthesiologica Scandinavica*, vol. 62, no. 9, pp. 1200–1208, 2018.

[19] M. Elvekjaer, E. K. Aasvang, R. M. Olsen, H. B. Sørensen, C. M. Porsbjerg, J. U. Jensen, C. Haahr-Raunkjær, and C. S. Meyhoff, "Physiological abnormalities in patients admitted with acute exacer-

bation of COPD: an observational study with continuous monitoring," *Journal of Clinical Monitoring and Computing*, 2019.

[20] R. M. Olsen, E. K. Aasvang, C. S. Meyhoff, and H. B. Dissing Sorensen, "Towards an automated multimodal clinical decision support system at the post anesthesia care unit," *Computers in Biology and Medicine*, vol. 101, no. May, pp. 15–21, 2018.

[21] J. E. Hall and A. C. Guyton, *Textbook of Medical Physiology*, 12th ed. Saunders, Elsevier, 2006.

[22] X. Ding, B. P. Yan, Y. T. Zhang, J. Liu, N. Zhao, and H. K. Tsang, "Pulse Transit Time Based Continuous Cuffless Blood Pressure Estimation: A New Extension and A Comprehensive Evaluation," *Scientific Reports*, vol. 7, no. 1, pp. 1–11, 2017.

[23] B. S. Alpert, D. Quinn, and D. Gallick, "Oscillometric blood pressure: a review for clinicians," *Journal of the American Society of Hypertension*, vol. 8, no. 12, p. 930–938, 2014.

[24] B. Silke and D. Mcauley, "Accuracy and precision of blood pressure determination with the finapres: an overview using re-sampling statistics," *Journal of Human Hypertension*, vol. 12, no. 6, p. 403–409, 1998.

[25] J. Allen, "Photoplethysmography and its application in clinical physiological measurement," *Physiological Measurement*, vol. 28, no. 3, 2007.

[26] N. Sviridova and K. Sakai, "Human photoplethysmogram: new insight into chaotic characteristics," *Chaos, Solitons & Fractals*, vol. 77, p. 53–63, 2015.

[27] J. Proença, J. Muehlsteff, X. Aubert, and P. Carvalho, "Is pulse transit time a good indicator of blood pressure changes during short physical exercise in a young population?" *2010 Annual International Conference of the IEEE Engineering in Medicine and Biology*, 2010.

[28] B. M. McCarthy, C. J. Vaughan, B. O'Flynn, A. Mathewson, and C. Ó. Mathúna, "An examination of calibration intervals required for accurately tracking blood pressure using pulse transit time algorithms," *Journal of Human Hypertension*, vol. 27, no. 12, pp. 744–750, 2013.

[29] X. R. Ding, Y. T. Zhang, J. Liu, W. X. Dai, and H. K. Tsang, "Continuous Cuffless Blood Pressure Estimation Using Pulse Transit Time and Photoplethysmogram Intensity Ratio," *IEEE Transactions on Biomedical Engineering*, vol. 63, no. 5, pp. 964–972, 2016.

[30] M. Radha, K. De Groot, N. Rajani, C. C. Wong, N. Kobold, V. Vos, P. Fonseca, N. Mastellos, P. A. Wark, N. Velthoven, R. Haakma, and R. M. Aarts, "Estimating blood pressure trends and the nocturnal dip from photoplethysmography," *Physiological Measurement*, vol. 40, no. 2, pp. 1–20, 2019.

[31] J. C. Ruiz-Rodríguez, A. Ruiz-Sanmartín, V. Ribas, J. Caballero, A. García-Roche, J. Riera, X. Nuvials, M. De Nadal, O. De Sola-Morales, J. Serra, and J. Rello, "Innovative continuous non-invasive cuffless blood pressure monitoring based on photoplethysmography technology," *Intensive Care Medicine*, vol. 39, no. 9, pp. 1618–1625, 2013.

[32] Y. Kurylyak, F. Lamonaca, and D. Grimaldi, "A Neural Network-based method for continuous blood pressure estimation from a PPG signal," *Conference Record - IEEE Instrumentation and Measurement Technology Conference*, pp. 280–283, 2013.

[33] G. S. Stergiou, B. Alpert, S. Mieke, R. Asmar, N. Atkins, S. Eckert, G. Frick, B. Friedman, T. Graßl, T. Ichikawa, J. P. Ioannidis, P. Lacy, R. McManus, A. Murray, M. Myers, P. Palatini, G. Parati, D. Quinn, J. Sarkis, A. Shennan, T. Usuda, J. Wang, C. O. Wu, and E. O'Brien, "A universal standard for the validation of blood pressure measuring devices: Association for the Advancement of Medical Instrumentation/European Society of Hypertension/International Organization for Standardization (AAMI/ESH/ISO) Collaboration Statement," *Hypertension*, vol. 71, no. 3, pp. 368–374, 2018.

[34] E. O'Brien, J. Petrie, W. Littler, M. De Swiet, P. L. Padfield, K. O'Malley, M. Jamieson, D. Altman, M. Bland, and N. Atkins, "The british hypertension society protocol for the evaluation of automated and semi-automated blood pressure measuring devices with special reference to ambulatory systems," *Journal of Hypertension*, vol. 8, no. 7, pp. 607–619, 1990.

[35] S. S. Mousavi, M. Firouzmand, M. Charmi, M. Hemmati, M. Moghadam, and Y. Ghorbani, "Blood pressure estimation from appropriate and inappropriate PPG signals using A whole-based method," *Biomedical Signal Processing and Control*, vol. 47, pp. 196–206, 2019.

[36] L. Wang, W. Zhou, Y. Xing, and X. Zhou, "A novel neural network model for blood pressure estimation using photoplethesmography without electrocardiogram," *Journal of Healthcare Engineering*, vol. 2018, 2018.

[37] G. Thambiraj, U. Gandhi, V. Devanand, and U. Mangalanathan, "Noninvasive cuffless blood pressure estimation using pulse transit time, Womersley number, and photoplethysmogram intensity ratio," *Physiological Measurement*, vol. 40, no. 7, 2019.

[38] P. Su, X. R. Ding, Y. T. Zhang, J. Liu, F. Miao, and N. Zhao, "Long-term blood pressure prediction with deep recurrent neural networks," *2018 IEEE EMBS International Conference on Biomedical and Health Informatics, BHI 2018*, vol. 2018-Janua, pp. 323–328, 2018.

[39] M. S. Tanveer and M. K. Hasan, "Cuffless blood pressure estimation from electrocardiogram and photoplethysmogram using waveform based ANN-LSTM network," *Biomedical Signal Processing and Control*, vol. 51, pp. 382–392, 2019.

[40] W.-H. Lin, H. Wang, O. W. Samuel, G. Liu, Z. Huang, and G. Li, "New photoplethysmogram indicators for improving cuffless and continuous blood pressure estimation accuracy," *Physiological Measurement*, vol. 39, no. 2, p. 025005, 2018.

[41] X. Xing and M. Sun, "Optical blood pressure estimation with photoplethysmography and fft-based neural networks," *Biomedical Optics Express*, vol. 7, no. 8, p. 3007, 2016.

[42] I. Sharifi, S. Goudarzi, and M. B. Khodabakhshi, "A novel dynamical approach in continuous cuffless blood pressure estimation based on ECG and PPG signals," *Artificial Intelligence in Medicine*, vol. 97, no. April 2018, pp. 143–151, 2019.

[43] Y. Chen, S. Shi, Y. K. Liu, S. L. Huang, and T. Ma, "Cuffless blood-pressure estimation method using a heart-rate variability-derived parameter," *Physiological Measurement*, vol. 39, no. 9, 2018.

[44] W. Lin, H. Wang, O. W. Samuel, and G. Li, "Using a new ppg indicator to increase the accuracy of ptt-based continuous cuffless blood pressure estimation," in *2017 39th Annual International Conference of the IEEE Engineering in Medicine and Biology Society (EMBC)*, 2017, pp. 738–741.

[45] S. G. Khalid, J. Zhang, F. Chen, and D. Zheng, "Blood pressure estimation using photoplethysmography only: Comparison between different machine learning approaches," *Journal of Healthcare Engineering*, vol. 2018, p. 1–13, 2018.

[46] G. D. Clifford, D. J. Scott, and M. Villarroel, "User guide and documentation for the MIMIC II database," *MIMIC-II database version*, vol. 2, no. January 2009, 2009.

[47] "wavelet signal denoising - matlab." [Online]. Available: https://www.mathworks.com/help/wavelet/ref/wdenoise.html

[48] M. Elgendi, "Optimal signal quality index for photoplethysmogram signals," *Bioengineering*, vol. 3, no. 4, pp. 1–15, 2016.

[49] F. Scholkmann, J. Boss, and M. Wolf, "An efficient algorithm for automatic peak detection in noisy periodic and quasi-periodic signals," *Algorithms*, vol. 5, no. 4, pp. 588–603, 2012.

[50] T. Hastie, J. Friedman, and R. Tisbshirani, *The Elements of statistical learning: data mining, inference, and prediction*. Springer, 2017.

[51] L. Breiman, "Random forests," *Machine Learning*, vol. 45, p. 5–32, 2001.

[52] E. Monte-Moreno, "Non-invasive estimate of blood glucose and blood pressure from a photoplethysmograph by means of machine learning techniques," *Artificial Intelligence in Medicine*, vol. 53, no. 2, p. 127–138, 2011.

[53] G. Slapni Č Ar, N. Mlakar, and M. Luštrek, “Blood pressure estimation from photoplethysmogram using a spectro-temporal deep neural network,” *Sensors (Switzerland)*, vol. 19, no. 15, 2019.

[54] M. Elgendi, “C , E and D Waves Detection in the Acceleration Photoplethysmogram,” *Computer Methods and Programs in Biomedicine*, vol. 117, no. 2, pp. 125–136, 2014.